A Three-Phase Inverter Based Overmodulation Strategy of Asymmetrical Six-Phase Induction Machine

Sayan Paul and Kaushik Basu, *Senior Member, IEEE*

***Abstract*—Overmodulation (OVM) techniques of asymmetrical six-phase induction machine (ASIM) achieve higher dc-bus utilization by applying nonzero average voltage in nonenergy transfer plane. This results into unwanted current and associated copper loss. Existing OVM techniques reduce this loss with pulsewidth modulation (PWM) techniques from six-dimensional space vector perspective, which is both conceptually difficult and computationally challenging. The computational complexity of space vector based techniques is reduced by few existing PWM techniques in linear region by splitting the six-phase inverter as two three-phase inverters and modulate these inverters with linear PWM techniques in 30° phase shifted. This is referred as three-phase inverter based technique in the title. But, three-phase inverter based OVM technique does not exist in the literature due to lack of knowledge of the relationship between six-dimensional space vectors and space vectors of two three-phase inverters. This article first establishes this relation. Based on this relation, an OVM technique is proposed where the reference voltage vectors of two inverters are phase shifted by 30° but of different magnitudes. The proposed technique achieves THD and WTHD performances similar to space vector based best technique of ASIM with reduced computational complexity, as shown in details. The proposed strategy is validated through experiments and simulations on six-phase induction machine at 4.2 kW.**

***Index Terms*—Asymmetrical six-phase induction motor (ASIM), harmonic minimization, multiphase machines, overmodulation (OVM), pulsewidth modulation (PWM), six-phase drives.**

I. Introduction

ASYMMETRICAL six-phase induction machine (ASIM) is one of the most common multiphase machines, which is preferred over conventional three-phase (3ϕ) machine in high power applications due to advantages, such as better fault tolerance for having phase redundancy, lower space harmonic content, less susceptibility toward excitation harmonics, and reduced rating of the power electronic components compared to three-phase machine [1], [2]. Fig. 1 shows the six-phase windings of ASIM where the six windings can be seen as two sets of balanced 3ϕ windings and the spatial shift between these two sets is 30° electrical. Due to this winding structure, 6th, 18th, $12k+6$, $k=0,1,\ldots$ order harmonic torques cannot be produced even with nonsinusoidal excitation [3]. This fact makes ASIM advantageous over symmetrical six phase where all six windings are symmetrically displaced by 60°. Significant amount of research has been done over last few decades to thoroughly investigate ASIM modeling and design [4]–[6], pulsewidth modulation (PWM) techniques [3], [6]–[17], different control strategies [18], [19], and fault tolerant operation [20]–[22].

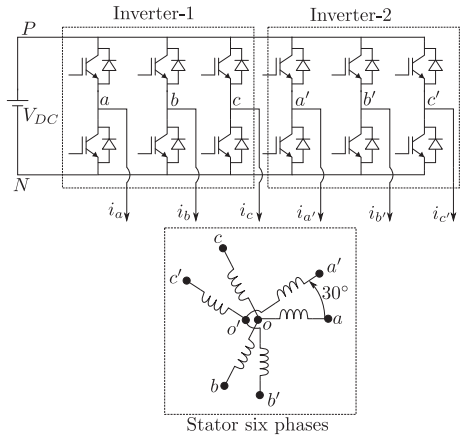

Fig. 1. Six-phase inverter fed ASIM.

Dynamic model of ASIM had been derived in multiple ways in the existing literature, such as double *d–q* theory [23] and vector space decomposition (VSD) theory [6]. The later one is the most popular way to model ASIM and the modulation strategy proposed in this article is based on this theory. A 6×6 transformation matrix T was proposed in VSD theory to model the 6-D ASIM. T transforms 6-D quantities from original frame to three 2-D orthogonal subspaces. It is shown in [6] that one of the subspaces, namely $\alpha-\beta$, is solely responsible for electromagnetic energy transfer. The two 2-D subspaces, which are not associated with energy transfer, have been labeled as z_1-z_2 and o_1-o_2 in this article. The impedance of z_1-z_2 and o_1-o_2 subspaces is small as it consists of winding resistance and leakage inductance. As $\alpha-\beta$ is associated with energy transfer, this subspace should be excited with balanced fundamental

Manuscript received April 10, 2020; revised August 1, 2020; accepted September 16, 2020. Date of publication September 25, 2020; date of current version January 22, 2021. This work was supported by the Department of Science and Technology, Government of India, under the project titled "Development of an Advanced System-On-Chip (SoC) Based Embedded Controller for Power Electronic Converters." Recommended for publication by Associate Editor M. Tavakoli Bina. *(Corresponding author: Sayan Paul.)*

The authors are with the Department of Electrical Engineering, Indian Institute of Science, Bangalore 560012, India (e-mail: sayanp@iisc.ac.in; basux017@umn.edu).

Color versions of one or more of the figures in this article are available online at https://ieeexplore.ieee.org.

Digital Object Identifier 10.1109/TPEL.2020.3026816

voltage in order to generate ripple-free torque in ASIM. With the balanced winding with two isolated neutrals, as shown in Fig. 1, $o_1 - o_2$ plane cannot be excited. Although applied voltage in $z_1 - z_2$ does not create torque ripple, it causes large circulating current and associated copper loss due to low impedance of the equivalent circuit. Therefore, applied voltage in $z_1 - z_2$ should be as small as possible. Linear modulation techniques of ASIM do not inject any voltage in $z_1 - z_2$, whereas the overmodulation (OVM) techniques do inject some voltage in $z_1 - z_2$ in order to extend the region in $\alpha - \beta$ plane available for modulation.

Linear PWM techniques of ASIM can be broadly classified into two categories: First, 4-D space vector based PWM techniques, where at least four active vectors along with the zero vector are used within a sampling period in order to generate reference voltage vector in $\alpha - \beta$ and zero average voltage vector in $z_1 - z_2$ plane [6]–[11]. Here, one technique differs from others in terms of current ripple performances. Second, two 3ϕ inverter (TINV) based PWM techniques, as proposed in [15] and [16], where the 6ϕ inverter is split into TINVs, inverter-1 and inverter-2 of Fig. 1. Inverter-1 is modulated with half of the reference voltage vector in $\alpha - \beta$ plane. Reference vector of inverter-2 is of same magnitude that of inverter-1 but phase shifted by 30°. The second category of techniques, i.e., TINV techniques, are referred as three-phase inverter based technique in the title of this article. Carrier comparison based implementation of TINV techniques is computationally less burdened compared to implementation of space vector based techniques where complex 6-D transformation is involved. Modulation index (M) is defined as the ratio of the peak of the fundamental component of the line to neutral voltage to the dc-bus voltage. The maximum M achievable by both of these categories of techniques is 0.577.

OVM of PWM converter is important for higher dc bus utilization and reduction in voltage rating of the switching devices and to meet higher voltage requirement during transients and peak loading conditions [24]. OVM of multiphase machines is interesting because unlike the three-phase case, there is no torque pulsation here. OVM of five-phase machines has been widely discussed in the literature [25]–[29]. OVM techniques of ASIM extend the range of M up to 0.622 by applying nonzero average voltage in $z_1 - z_2$ plane. But, rms voltage injected in this plane should be small in order to have small resultant current and associated copper loss. Gopakumar *et al.* [3] and Zhou *et al.* [10] proposed 4-D space vector based OVM techniques. The proposed technique in [3], later named as *CSVPWM* in [6], uses two large active vectors adjacent to reference voltage vector in $\alpha - \beta$ and it injects substantial amount of harmonic voltages in $z_1 - z_2$ plane. To reduce this rms voltage injection, Zhou *et al.* [10] has proposed two OVM algorithms, which are labeled as *SVOVM4-1* and *SVOVM4-2*, respectively, in this article. These techniques use two large and two medium active vectors adjacent to reference voltage vector in $\alpha - \beta$ plane. *SVOVM4-2* is the best known OVM technique in ASIM literature. One should notice that both five-phase machine with one isolated neutral and ASIM with two isolated neutrals require 4-D modulation. 4-D space vector based OVM techniques for five-phase machines are available in [25], [27], and [28].

But TINV-based OVM techniques are an open problem in ASIM literature. Although Yazdani *et al.* [17] have applied standard 3ϕ OVM techniques, as proposed by Holtz *et al.* [30], on individual 3ϕ inverters in 30° phase-shifted way, this technique injects harmonic voltages in $\alpha - \beta$, which in turn causes low-frequency torque pulsations violating OVM condition of ASIM. In this article, a TINV-based OVM technique is proposed, which can be implemented with reduced computational complexity, as TINV-based linear techniques, and without compromising on the performance of the drive. Following are the contributions of this article.

1) In order to analyze OVM from TINV perspective, a key relation between the six-phase quantities, obtained using the transformation defined in [6], with three-phase quantities, obtained through familiar $3\phi - 3\phi$ Clarke's transformation, is derived. This relationship is new to the literature.
2) Using that relationship, a TINV-based OVM technique of ASIM is proposed. This technique split the reference voltage vector in $\alpha - \beta$ plane into two reference voltage vectors of TINVs such that they are phase shifted by 30° and of different magnitudes in OVM region but of same magnitude in linear region. The proposed strategy works up to $M = 0.5977$. It attains voltage total harmonic distortion (THD) performance almost similar to *SVOVM4-2*.
3) A detailed comparison of computational burdens between the TINV-based proposed technique and 4-D space vector based *SVOVM4-2* shows that the proposed technique can be implemented at much reduced computational cost without involving complex 6-D transformation.

The organization of this article is as follows. Section II briefly discusses about the modeling of ASIM. Section III discusses the existing modulation techniques. The important relationships between three-phase and six-phase space vectors and an OVM technique based on the aforementioned relationship are presented in Sections IV and V, respectively. The implementation strategy, and simulation and experimental results, are discussed in Sections VI and VII, respectively. Finally, Section VIII concludes the article.

II. Dynamic Model of ASIM

$$X_i \triangleq \underbrace{\frac{1}{\sqrt{3}}\begin{bmatrix} 1 & -\frac{1}{2} & -\frac{1}{2} & \frac{\sqrt{3}}{2} & -\frac{\sqrt{3}}{2} & 0 \\ 0 & \frac{\sqrt{3}}{2} & -\frac{\sqrt{3}}{2} & \frac{1}{2} & \frac{1}{2} & -1 \\ 1 & -\frac{1}{2} & -\frac{1}{2} & -\frac{\sqrt{3}}{2} & \frac{\sqrt{3}}{2} & 0 \\ 0 & -\frac{\sqrt{3}}{2} & \frac{\sqrt{3}}{2} & \frac{1}{2} & \frac{1}{2} & -1 \\ 1 & 1 & 1 & 0 & 0 & 0 \\ 0 & 0 & 0 & 1 & 1 & 1 \end{bmatrix}}_{T} X_j$$

$$X_i = X_{\alpha\beta z_1 z_2 o_1 o_2} = \begin{bmatrix} x_\alpha & x_\beta & x_{z_1} & x_{z_2} & x_{o_1} & x_{o_2} \end{bmatrix}^T$$

$$X_j = X_{abca'b'c'} = \begin{bmatrix} x_a & x_b & x_c & x_{a'} & x_{b'} & x_{c'} \end{bmatrix}^T. \quad (1)$$

As six windings of ASIM can be excited from six independent voltage or current sources, ASIM is 6-D. A 6×6 orthonormal transformation matrix T, given in (1), has been used in [6] for analyzing the dynamic model of ASIM. The co-ordinates in original and transformed domains are labeled as $a-b-c-a'-b'-c'$ and $\alpha-\beta-z_1-z_2-o_1-o_2$, respectively. Here, X is a 6-D vector whose element x represents the machine variables, such as voltage, current, flux linkage, etc.

A six-phase inverter fed squirrel-cage ASIM is shown in Fig. 1, where the six-phase inverter can be identified as two three-phase inverters, inverter-1 and inverter-2, respectively. The terminals of the six stator phase windings are a, b, c, a', b', c', which are directly connected to the poles of the six legs of the inverter. These two sets of balanced three-phase windings are connected in star fashion and they form two isolated neutral points, o and o'. Therefore, voltages impressed on o_1-o_2 plane by any of the switching state of this particular configuration will be zero (as the last two rows of T give the zero-sequence components of two sets of three-phase line neutral voltages). So, discussions in the subsequent sections are focused to generate desired output voltages in $\alpha-\beta$ and z_1-z_2 subspaces

$$\begin{aligned}\vec{\psi}_{s,\alpha\beta} &= L_s\vec{i}_{s,\alpha\beta} + L_M e^{j\theta_r}\vec{i}_{r,\alpha\beta}; \qquad \vec{\psi}_{s,z_1z_2} = L_{ls}\vec{i}_{s,z_1z_2}\\ \vec{\psi}_{r,\alpha\beta} &= L_M e^{-j\theta_r}\vec{i}_{s,\alpha\beta} + L_r\vec{i}_{r,\alpha\beta}; \qquad \vec{\psi}_{r,z_1z_2} = L_{lr}\vec{i}_{r,z_1z_2}\end{aligned} \tag{2}$$

$$\vec{v}_{k,\alpha\beta/z_1z_2} = r_k\vec{i}_{k,\alpha\beta/z_1z_2} + \frac{d}{dt}\vec{\psi}_{k,\alpha\beta/z_1z_2}; \quad k=s,r \tag{3}$$

The machine model in $\alpha-\beta$ and z_1-z_2 subspaces, as obtained by Zhao and Lipo [6], are given in (2) and (3). Here, $\vec{\psi}_{s,\alpha\beta} = \psi_{s\alpha} + j\psi_{s\beta}$; $\psi_{s\alpha}$ and $\psi_{s\beta}$ are stator flux linkages in α and β domains, respectively. Similarly, other quantities of (2) and (3) can be interpreted. $L_s - L_M = L_{ls}$; $L_r - L_M = L_{lr}$. Subscripts s and r are used to denote stator and rotor quantities, respectively. Following are few assumptions made during this modeling sinusoidal winding distribution, infinite permeability of iron, linear, and unsaturated magnetic material, and uniform air-gap between stator and rotor. Three important properties of this model are outlined as follows.

1) Six subspaces in transformed domain are orthogonal to each other and can be grouped into three 2-D subspaces, viz., $\alpha-\beta$, z_1-z_2, and o_1-o_2, respectively. The dynamical equations of ASIM in these three subspaces can be analyzed independently due to their decoupled nature.
2) The mutual coupling between the stator and rotor windings appear only in $\alpha-\beta$ subspace. From this, it can be concluded that only $\alpha-\beta$ subspace is associated with electromechanical energy conversion and torque production. Both the dynamical and steady-state equivalent circuits in this subspace are similar to the equivalent circuits of three-phase induction machine (IM) with 3ϕ Clarke's transformation.
3) The flux linkages in z_1-z_2 and o_1-o_2 subspaces have no coupling between stator and rotor, as if air-gap flux does not appear in these subspaces. The equivalent circuits in these subspaces have winding resistance and leakage inductance. As the impedances of these equivalent circuits are small, any voltage applied in these subspaces causes large current resulting into copper losses and this large current does not contribute in electromagnetic energy conversion or torque pulsation.

From the aforementioned discussion, it is clear that the excitation of $\alpha-\beta$ plane with balanced fundamental voltage will result into operation of ASIM similar to 3ϕ IM without creating any torque ripple. The voltage excitations in z_1-z_2 and o_1-o_2 subspaces should be zero or as small as possible in order to drive ASIM efficiently. Although the sinusoidal winding distribution is an ideal assumption, which is not the case in practical, space harmonics of nonsinusoidal winding distribution can be neglected as the mutual inductance due to nth harmonic falls rapidly, as $\frac{1}{n^2}$ [31]. Incorporation of mutual leakage inductance in the dynamic modeling does not change the key properties, as listed above from 1) to 3) [4].

III. Existing Modulation Techniques

A brief review of existing modulation techniques of asymmetrical six-phase inverter drives is presented in this section. These modulation techniques can be broadly classified into two categories: linear modulation techniques and OVM techniques. To avoid the unnecessary copper loss, average voltage in z_1-z_2 plane is kept zero in linear modulation region. In OVM region, fundamental voltage in $\alpha-\beta$ is increased at the cost of applying nonzero voltage in z_1-z_2 plane. As no harmonic is injected in $\alpha-\beta$, there is no torque pulsation in OVM region. The main objective of the OVM techniques is to reduce rms current in z_1-z_2 plane to reduce the copper loss.

A. Linear Modulation Region

The modulation problem in linear region can be approached in two ways: two inverter (TINV) and space vector (SVPWM) approaches.

1) TINV Techniques: Let the controller provides $\overline{v}_\alpha$ and $\overline{v}_\beta$, average reference voltages in $\alpha-\beta$ plane or reference voltage vector in $\alpha-\beta$ ($\vec{V}_{\text{ref}}$), which is given as follows:

$$\vec{V}_{\text{ref}} \triangleq \overline{v}_\alpha + j\overline{v}_\beta. \tag{4}$$

In linear range, $\overline{v}_{z_1} = \overline{v}_{z_2} = 0$. Here, bar represents the average voltage over a switching cycle. Due to isolated neutral connections, $\overline{v}_{o_1} = \overline{v}_{o_2} = 0$. By taking inverse transformation (T^{-1}) on these transformed domain voltages, the average line-neutral voltages $\overline{v}_{io}$ and $\overline{v}_{i'o'}$, $i = a, b, c$, are obtained. Based on these two sets of three-phase line-neutral voltages, two common mode voltages $\overline{v}_{oN}$ and $\overline{v}_{o'N}$ are chosen independently, N is dc-bus negative terminal, as shown in Fig. 1. The most popular choice of common mode voltage is $\frac{1}{2} + \frac{\text{mid}}{2}$, where mid is the middle value of the corresponding three average line-neutral voltages.

For balanced sinusoidal operation in steady state, suppose $\overline{v}_\alpha = \sqrt{3}V_o\cos(\omega_o t = \theta)$, $\overline{v}_\beta = \sqrt{3}V_o\sin\theta$, and $\overline{v}_{z_1} = \overline{v}_{z_2} = \overline{v}_{o_1} = \overline{v}_{o_2} = 0$. Therefore

$$\vec{V}_{\text{ref}} = \sqrt{3}V_o e^{j\theta} \tag{5}$$

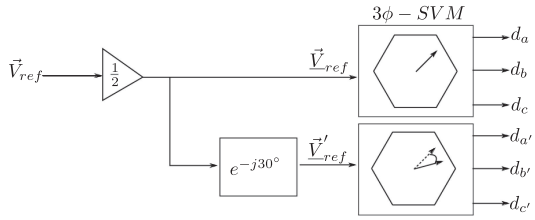

Fig. 2. Modulation of ASIM in linear region based on TINV strategy.

$$\overline{v}_{io} = V_o \cos\left(\theta - \frac{k_i 2\pi}{3}\right), \overline{v}_{i'o'} = V_o \cos\left(\theta - \left(\frac{\pi}{6} + \frac{k_i 2\pi}{3}\right)\right). \tag{6}$$

Applying T^{-1} on these transformed domain voltages, line-neutral voltages can be obtained as (6), where $i \in \{a, b, c\}$ and $k_a = 0, k_b = 1, k_c = 2$. These two sets are three-phase balanced sinusoidal voltages and they are phase shifted by 30° to each other. Equation (7a) defines 3ϕ Clarke transformation, where C relates $a - b - c$ to $\underline{\alpha} - \underline{\beta} - \underline{o}$. One should note here that $\underline{\alpha} - \underline{\beta}$ of 3ϕ is different from $\alpha - \beta$ of 6ϕ, underline is used to denote the three-phase transformed domain quantities. The reference voltage vectors of the two three-phase inverters are commonly defined as (8), where prime denotes the quantities related to second inverter. Plugging the balanced sinusoidal average line-neutral voltages of (6) in (7), the reference voltage vectors of the two inverters are obtained from the definition given in (8) as $\underline{\vec{V}}_{\text{ref}} = \frac{\sqrt{3}}{2} V_o e^{j\theta}$ and $\underline{\vec{V}}'_{\text{ref}} = \frac{\sqrt{3}}{2} V_o e^{j(\theta - 30^\circ)}$. One can also see that for balanced sinusoidal operation, $\underline{\vec{V}}_{\text{ref}} = \frac{\vec{V}_{\text{ref}}}{2}$ and $\underline{\vec{V}}'_{\text{ref}} = \frac{\vec{V}_{\text{ref}}}{2} e^{-j30^\circ}$

$$\underbrace{\begin{bmatrix} v_{\underline{\alpha}} \\ v_{\underline{\beta}} \\ v_{\underline{o}} \end{bmatrix}}_{V_{\underline{\alpha}\underline{\beta}\underline{o}}} \triangleq \underbrace{\frac{1}{\sqrt{3}} \begin{bmatrix} 1 & -\frac{1}{2} & -\frac{1}{2} \\ 0 & \frac{\sqrt{3}}{2} & -\frac{\sqrt{3}}{2} \\ 1 & 1 & 1 \end{bmatrix}}_{C} \underbrace{\begin{bmatrix} v_{ao} \\ v_{bo} \\ v_{co} \end{bmatrix}}_{V_{abc}} \tag{7a}$$

$$V_{\underline{\alpha'}\underline{\beta'}\underline{o'}} \triangleq C V_{a'b'c'}; \quad V_{a'b'c'} = \begin{bmatrix} v_{a'o'} & v_{b'o'} & v_{c'o'} \end{bmatrix}^T \tag{7b}$$

$$\underline{\vec{V}}_{\text{ref}} \triangleq \overline{v}_{\underline{\alpha}} + j\overline{v}_{\underline{\beta}}; \qquad \underline{\vec{V}}'_{ref} \triangleq \overline{v}_{\underline{\alpha'}} + j\overline{v}_{\underline{\beta'}}. \tag{8}$$

Therefore, it can be seen that modulation of ASIM in linear range can be performed from two three-phase inverters with reference voltage vectors of equal magnitude but phase shifted by 30° and reference voltage vector of one of the inverters is half of the reference voltage vector in $\alpha - \beta$ of 6ϕ machine. This is illustrated in Fig. 2 where d_i represents the duty ratio of the top switch of ith leg. Here, transformation matrix T is not required. Based on the aforementioned idea, modulation techniques, such as double zero-sequence injection technique ([16]), three waves based zero-sequence injection PWM, and six waves based zero-sequence injection PWM ([12]), have been proposed. If modulation index (M) is defined as the ratio of peak line-neutral fundamental voltage and dc-bus voltage, i.e., $M = \frac{V_o}{V_{\text{DC}}}$, maximum M of asymmetrical six-phase drive in linear region is 0.577.

2) SVPWM Techniques: In this technique, voltages generated by 64 switching states of the six-phase inverter are mapped into $\alpha - \beta$ and $z_1 - z_2$ subspaces using T. This mapping results into 60 active vectors and 4 zero vectors in both $\alpha - \beta$ and $z_1 - z_2$ subspaces [6], [12], [17]. Using these switching vectors, the desired reference voltage vectors in these subspaces are synthesized. In linear region, reference voltage vectors in $\alpha - \beta$ are given by (5) and (9) give the reference voltages in $z_1 - z_2$

$$\overline{v}_{z_1} + j\overline{v}_{z_2} = 0. \tag{9}$$

To satisfy the four constraints of (5) and (9), minimum four active states have to be applied along with zero states. These four active vectors can be chosen in multiple ways. Depending upon the choice of vectors, different modulation techniques exist in the literature, such as VSD technique in [6], 24-sector VSD in [8], modified 24-sector VSD in [11] and [13], and four vector technique with two large and two medium vectors in [9] and [10]. It is possible to show that all of these techniques can attain maximum M equal to 0.577 in linear region.

It is clear from the aforementioned discussion that with TINV techniques, one can modulate ASIM from the knowledge of two-level three-phase VSI without involving complicated 6-D transformation T. But unlike TINV, SVPWM techniques require knowledge of T and this makes it both conceptually and computationally challenging compared to TINV techniques.

B. OVM Region

As $M > 0.577$ in OVM region, the six-phase inverter will inject harmonics in line-neutral voltages, which appear only in $z_1 - z_2$ plane but not in $\alpha - \beta$. Therefore, at the outset, $\overline{v}_\alpha$ and $\overline{v}_\beta$ are known as before (coming from the controller), but $\overline{v}_{z_1}$ and $\overline{v}_{z_2}$ are not known. Therefore, all of the OVM techniques try to define $\overline{v}_{z_1}$ and $\overline{v}_{z_2}$ by adopting different strategies

$$\begin{aligned} v_\alpha &= \frac{1}{\sqrt{3}} \left(\left(v_{ao} - \frac{v_{bo}}{2} - \frac{v_{co}}{2} \right) + \frac{\sqrt{3}}{2} \left(v_{a'o'} - v_{b'o'} \right) \right) \\ &= \left(v_{\underline{\alpha}} + \frac{1}{2} \left(v_{a'o'} - v_{b'o'} \right) \right) \end{aligned} \tag{10}$$

$$\begin{aligned} v_\beta &= \frac{1}{\sqrt{3}} \left(\frac{\sqrt{3}}{2} \left(v_{bo} - v_{co} \right) - \left(v_{c'o'} - \frac{v_{b'o'}}{2} - \frac{v_{a'o'}}{2} \right) \right) \\ &= \left(v_{\underline{\beta}} - \frac{1}{\sqrt{3}} \left(v_{c'o'} - \frac{v_{b'o'}}{2} - \frac{v_{a'o'}}{2} \right) \right) \end{aligned} \tag{11}$$

$$\begin{aligned} v_\alpha + j v_\beta = &\left(v_{\underline{\alpha}} + j v_{\underline{\beta}} \right) \\ &+ \frac{1}{\sqrt{3}} \underbrace{\left(\frac{\sqrt{3}}{2} \left(v_{a'o'} - v_{b'o'} \right) - j \left(v_{c'o'} - \frac{v_{b'o'}}{2} - \frac{v_{a'o'}}{2} \right) \right)}_{\mathbb{V}_u} \end{aligned} \tag{12}$$

$$\begin{aligned} \mathbb{V}_u = &\left(\left(v_{a'o'} - \frac{v_{b'o'}}{2} - \frac{v_{c'o'}}{2} \right) + j \frac{\sqrt{3}}{2} \left(v_{b'o'} - v_{c'o'} \right) \right) \\ &\times \left(\frac{\sqrt{3}}{2} + j \frac{1}{2} \right) = \sqrt{3} \left(v_{\underline{\alpha'}} + j v_{\underline{\beta'}} \right) e^{j30^\circ}. \end{aligned} \tag{13}$$

1) SVPWM Techniques: Gopakumar *et al.* [3] proposed a strategy (which later named as *CSVPWM* in [6]) that uses two largest active vectors adjacent to the reference voltage vector in $\alpha-\beta$ plane in order to satisfy (5). Although this technique attains maximum M up to 0.622, it applies significant amount of voltage in z_1-z_2 plane. To reduce this applied voltage, Zhou *et al.* [10] have proposed two OVM algorithms, which are termed as *SVOVM4-1 (space vector based OVM technique-1 with four active vectors)* and *SVOVM4-2* in this article, with the following assumptions.

1) These techniques use four active vectors. These four vectors form two sets of vectors 30° apart in $\alpha-\beta$ plane. Each set comprises one large and one medium active vectors of $\alpha-\beta$ plane, which are along the same direction in $\alpha-\beta$ and 180° apart in z_1-z_2.
2) No zero vector is applied.

With the aforementioned choice of vectors, *SVOVM4-2* has optimized the length of the applied average voltage vector in z_1-z_2 plane.

2) TINV Techniques: Yazdani *et al.* [17] have extended the idea of two inverter based modulation by operating individual three-phase inverters through OVM schemes proposed in [30], where the second 3ϕ inverter follows the first inverter at a phase lag of 30° with respect to fundamental frequency. But these OVM schemes inject harmonics in $\alpha-\beta$ plane and results into torque pulsation. Therefore, no two inverter based OVM technique exists in the literature.

To suggest an OVM strategy based on two inverter approach, one needs to relate the six-phase transformed domain quantities with three-phase transformed domain quantities. We can see from (8) that for sinusoidal operation in linear range, $\overline{v}_\alpha + j\overline{v}_\beta \triangleq \vec{V}_{\text{ref}} = \underline{\vec{V}}_{\text{ref}} + \underline{\vec{V}}'_{\text{ref}} e^{j30^\circ}$.

1) Does this relation hold in general?
2) Can we write the reference voltage vector in z_1-z_2 plane in terms of $\overline{v}_{\underline{\alpha}} + j\overline{v}_{\underline{\beta}}$ and $\overline{v}_{\underline{\alpha}'} + j\overline{v}_{\underline{\beta}'}$?

These questions are answered in the next section by proposing an alternative way of modeling the asymmetrical six-phase inverter.

IV. Relationship Between Three-Phase and Six-Phase Space Vectors

In (7a) and (7b), each of the two sets of three-phase voltages have been transformed individually to $\underline{\alpha}\underline{\beta}\underline{o}$ and $\underline{\alpha}'\underline{\beta}'\underline{o}'$ using well-known Clarke's $3\phi-3\phi$ transformation C. Now, we will try to relate $V_{\alpha\beta z_1 z_2 o_1 o_2}$ with $V_{\underline{\alpha}\underline{\beta}\underline{o}}$ and $V_{\underline{\alpha}'\underline{\beta}'\underline{o}'}$. Using (1), (7a), and (7b) for voltage quantities, we can write (10) and (11). Then, combining (10) and (11), we get (12). The under-bracketed term in right-hand side of (12), $\mathbb{V}_u$, is simplified and expressed compactly in (13). Using (12) and (13), one gets the key expression (14a). Similarly, combining v_{z_1} and v_{z_2} using (1), (7a), (7b), and (13), one gets another important expression (14b). Here, * is complex conjugate operation. In (14c), o_1-o_2 quantities have been written in terms of zero sequence of the two three-phase inverters

$$v_\alpha + jv_\beta = \left(\left(v_{\underline{\alpha}} + jv_{\underline{\beta}}\right) + \left(v_{\underline{\alpha}'} + jv_{\underline{\beta}'}\right)e^{j30^\circ}\right) \tag{14a}$$

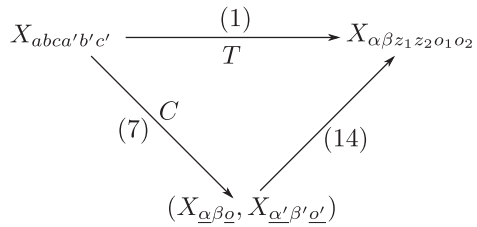

Fig. 3. Two ways to obtain quantities in transformed domains.

$$v_{z_1} + jv_{z_2} = \left(\left(v_{\underline{\alpha}} + jv_{\underline{\beta}}\right) - \left(v_{\underline{\alpha}'} + jv_{\underline{\beta}'}\right)e^{j30^\circ}\right)^* \tag{14b}$$

$$v_{o_1} + jv_{o_2} = v_{\underline{o}} + jv_{\underline{o}'}. \tag{14c}$$

Although the aforementioned relationship is shown for line-neutral voltages, it is true for other variables as well, such as current, flux linkage, etc. One can model ASIM with these 3ϕ space vectors and apply (14) to obtain the model in $\alpha-\beta$ and z_1-z_2. The resultant model is same as the model given in (2) and (3), as obtained by Zhao and Lipo [6]. Fig. 3 shows the two ways to obtain the transformed quantities from the quantities in original domain.

We had anticipated (14a) in previous section for average vectors in linear range. But here we can see that both (14a) and (14b) are true on an instantaneous basis. These two expressions are the key results where the complex vectors in $\alpha-\beta$ and z_1-z_2 are expressed as the linear combination of 3ϕ space vectors and their complex conjugates. These are essential for analysis of OVM of six-phase drive from two inverter perspective, as we will see in next section.

Two inverter based linear modulation techniques can be readily explained using aforementioned two expressions. If we take switching cycle average of (14a) and (14b), then combining these equations with average reference voltage vector equations of linear modulation techniques [(4), (8), and (9)], one can get $\underline{\vec{V}}_{\text{ref}} = \frac{\vec{V}_{\text{ref}}}{2}$ and $\underline{\vec{V}}'_{\text{ref}} = \frac{\vec{V}_{\text{ref}}}{2}e^{-j30^\circ}$.

V. Proposed OVM Technique

For the sake of convenience, two complex space vectors are defined as follows:

$$\mathbb{V}_1 \triangleq \left(v_{\underline{\alpha}} + jv_{\underline{\beta}}\right); \mathbb{V}_2 \triangleq \left(v_{\underline{\alpha}'} + jv_{\underline{\beta}'}\right)e^{j30^\circ}.$$

Taking switching cycle average on aforementioned equation and comparing with (8), one can see that $\overline{\mathbb{V}}_1 = \underline{\vec{V}}_{\text{ref}}$ and $\overline{\mathbb{V}}_2 = \underline{\vec{V}}'_{\text{ref}} e^{j30^\circ}$. With these new notations, reference voltage vectors in $\alpha-\beta$ and z_1-z_2 can be written as follows:

$$\vec{V}_{\text{ref}} = (\overline{\mathbb{V}}_1 + \overline{\mathbb{V}}_2) \tag{15a}$$

$$\overline{v}_{z_1} + j\overline{v}_{z_2} = (\overline{\mathbb{V}}_1 - \overline{\mathbb{V}}_2)^*. \tag{15b}$$

Each three-phase inverter of Fig. 1 has eight permissible switching states. Fig. 4 shows the voltage vectors generated by these switching states in $\underline{\alpha}-\underline{\beta}$ [following (7a) or (7b)]. Table I lists the labels used to identify the switching state of three-phase inverter. Each of these labels consists of three binary numbers corresponding to switching state of three legs, a, b and

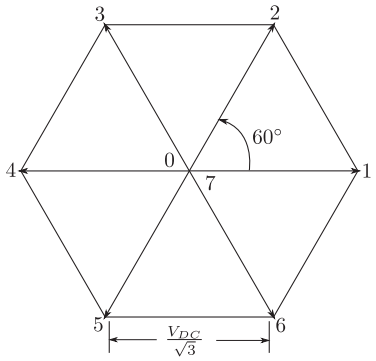

Fig. 4. Voltage vectors of three-phase inverter.

TABLE I
SWITCHING STATES OF THREE-PHASE INVERTER

Switching State	Label	Switching State	Label
000	0	011	4
100	1	001	5
110	2	101	6
010	3	111	7

c, respectively, in order. Here, 1 denotes that the top switch of a leg is "ON" and bottom switch is "OFF" and 0 denotes vice versa. The tips of six voltage vectors lie on the vertices of a regular hexagon and two states result into the zero vector, as shown in Fig. 4. It is possible to show that the tip of the average voltage space vectors generated by individual three-phase inverters ($\underline{\vec{V}}_{\text{ref}}$ and $\underline{\vec{V}}'_{\text{ref}}$) lie within this hexagon in order to satisfy the duty ratio constraints of the switches.

As $\overline{\mathbb{V}}_1 = \underline{\vec{V}}_{\text{ref}}$, $\overline{\mathbb{V}}_1$ will lie within hexagonal boundary as $\underline{\vec{V}}_{\text{ref}}$ and the boundary is shown in Fig. 5(a) with the label B_1. $\overline{\mathbb{V}}_2 = \underline{\vec{V}}'_{\text{ref}} e^{j30^\circ}$, therefore boundary of $\overline{\mathbb{V}}_2$, B_2, is obtained by rotating the hexagonal boundary of $\underline{\vec{V}}'_{\text{ref}}$ by 30°, as shown in Fig. 5(a). The length of the sides of these two hexagons is $\frac{V_{\text{DC}}}{\sqrt{3}}$. For brevity, all the lengths are scaled with a factor of $\frac{1}{V_{\text{DC}}}$. Therefore, length of each side of these two hexagons becomes $\frac{1}{\sqrt{3}}$, as shown in Fig. 5(a). The outermost dodecagon D_1 in Fig. 5(a) is the largest dodecagon obtained from vector addition of all possible $\overline{\mathbb{V}}_1$ and $\overline{\mathbb{V}}_2$ lying within B_1 and B_2, respectively. Therefore, $\vec{V}_{\text{ref}}$ should lie within D_1 in accordance to (15a). In linear modulation range, both (9) and (15b) give $\overline{\mathbb{V}}_1 = \overline{\mathbb{V}}_2$. With this constraint, the maximum boundary of both $\overline{\mathbb{V}}_1$ and $\overline{\mathbb{V}}_2$ is the boundary of the intersection region of B_1 and B_2, which has a shape of regular dodecagon. This is shown in Fig. 5(a) by dotted blue line. D_2 is obtained by doubling this intersection region and, hence, tip of $\vec{V}_{\text{ref}}$ has to lie within D_2 in linear range. In OVM ($M > 0.577$), tip of $\vec{V}_{\text{ref}}$ will lie partially or fully in the region between D_1 and D_2.

The $\alpha - \beta$ plane consists of 12 equivalent sectors, as shown in Fig. 5(b). As the modulation in all of these 12 sectors will be similar, only sector-1 ($-15^\circ \le \theta \le 15^\circ$) is considered for discussion. The boundaries of $\overline{\mathbb{V}}_1$, $\overline{\mathbb{V}}_2$, and $\overline{\mathbb{V}}_1 + \overline{\mathbb{V}}_2$ in 0° to 15° and 0° to −15° are symmetric with respect to real axis and, therefore, discussion can be further restricted to 0° to 15°. Fig. 5(c) shows the zoomed version of part of Fig. 5(a) when $0^\circ \le \theta \le 15^\circ$. $OC = \frac{1}{\sqrt{3}}$, as C is the vertex of hexagon B_1. $\angle OCA = 60^\circ$, $\angle COA = 15^\circ$, $\therefore \angle OAC = 105^\circ$. Applying sine rule, we get

$$\frac{OC}{\sin \angle OAC} = \frac{OA}{\sin \angle OCA} \Rightarrow OA = \frac{1}{2\cos 15^\circ}.$$

As $\angle OBA = 90^\circ$, $OB = OA\cos 15^\circ = \frac{1}{2}$. $OE = 2 \times OB = 1$, as DE, part of D_2, is obtained by doubling each vector lying on the line AB. These lengths are indicated in Fig. 5(c). All variables in modulo sector (sector-1) will be labeled with subscript m.

In Fig. 5(c), $\overline{\mathbb{V}}_{1m} \in \Delta OAC$ and $\overline{\mathbb{V}}_{2m} \in \Delta OAB$, where line segments AC and AB belong to the boundaries B_1 and B_2, respectively. Let $\overline{\mathbb{V}}_{1m} = \rho_1 e^{j\phi_1}$ and $\overline{\mathbb{V}}_{2m} = \rho_2 e^{j\phi_2}$. In linear modulation range, $\overline{\mathbb{V}}_{1m} = \overline{\mathbb{V}}_{2m}$ implies $\rho_1 = \rho_2$ and $\phi_1 = \phi_2$. As the maximum abscissa $\overline{\mathbb{V}}_{2m}$ can have is $OB = \frac{1}{2}$, therefore, the maximum abscissa $\overline{\mathbb{V}}_{1m}$ can have is also $OB = \frac{1}{2}$ in case of $\overline{\mathbb{V}}_{1m} = \overline{\mathbb{V}}_{2m}$, which implies $\overline{\mathbb{V}}_{1m} + \overline{\mathbb{V}}_{2m}$ can have maximum abscissa as $OE = 1$. Thus, linear techniques allow us to realize any $\vec{V}_{\text{ref},m}$ whose tip lies within ΔODE, where DE is part of D_2. To realize any $\vec{V}_{\text{ref},m}$ so that its tip lies within quadrilateral $DEGF$, where abscissa is greater than 1, we cannot have both $\rho_1 = \rho_2$ and $\phi_1 = \phi_2$. So, let us keep $\phi_1 = \phi_2$ but $\rho_1 \ne \rho_2$. The area within quadrilateral $DEGF$, which can be utilized for modulation with this strategy, is determined as follows.

As $\phi_1 = \phi_2$, both $\overline{\mathbb{V}}_{1m}$ and $\overline{\mathbb{V}}_{2m}$ subtend same angle with respect to OG and suppose $\phi_1 = \phi_2 = \phi$. To find the maximum boundary achievable with this condition, let both $\overline{\mathbb{V}}_{1m}$ and $\overline{\mathbb{V}}_{2m}$ move along their boundary keeping $\phi_1 = \phi_2 = \phi$. These vectors ($\overline{\mathbb{V}}_{1b}$ and $\overline{\mathbb{V}}_{2b}$) are shown in Fig. 5(c). Subscript b stands for boundary value. In Fig. 5(c), $\overline{\mathbb{V}}_{1b} = OY$ and $\overline{\mathbb{V}}_{2b} = OX$. $\angle COY = \phi = \angle BOX . \therefore \angle OYC = 120^\circ - \phi$. Applying sine rule, we get

$$\frac{OC}{\sin \angle OYC} = \frac{OY}{\sin \angle OCY} \text{ and } OX = \frac{OB}{\cos \phi}$$

and therefore, the absolute values of $\overline{\mathbb{V}}_{1b}$ and $\overline{\mathbb{V}}_{2b}$ can be expressed as functions of ϕ as follows:

$$OY = \rho_{1b}(\phi) = \frac{1}{2\cos(30^\circ - \phi)}$$
$$OX = \rho_{2b}(\phi) = \frac{OB}{\cos\phi} = \frac{1}{2\cos\phi}. \quad (16)$$

Using (15a), the boundary of $\vec{V}_{\text{ref},m}$ ($\vec{V}_{\text{ref}b}$) in this strategy can be determined by taking summation of $\rho_{1b}(\phi)$ and $\rho_{2b}(\phi)$ for $0^\circ \le \phi \le 15^\circ$. This is shown in Fig. 5(c) where $\vec{V}_{\text{ref}b}(\phi) = \rho_b(\phi)e^{j\phi}$ moves along curve GD and $\rho_b(\phi) = \rho_{1b}(\phi) + \rho_{2b}(\phi)$. Therefore, in addition to ΔODE, the shaded region within $DEGF$ (DEG) can be used for modulation of ASIM in $\alpha - \beta$ plane. Clearly, $\rho_b(\phi = 0^\circ) = OG$ and $\rho_b(\phi = 15^\circ) = OD$. Fig. 6 plots $\rho_b(\phi)$ as function of ϕ for $0^\circ \le \phi \le 15^\circ$. It can be seen that $\rho_b(\phi)$ is monotonically decreasing function in this range, and therefore, OD is the minimum vector length

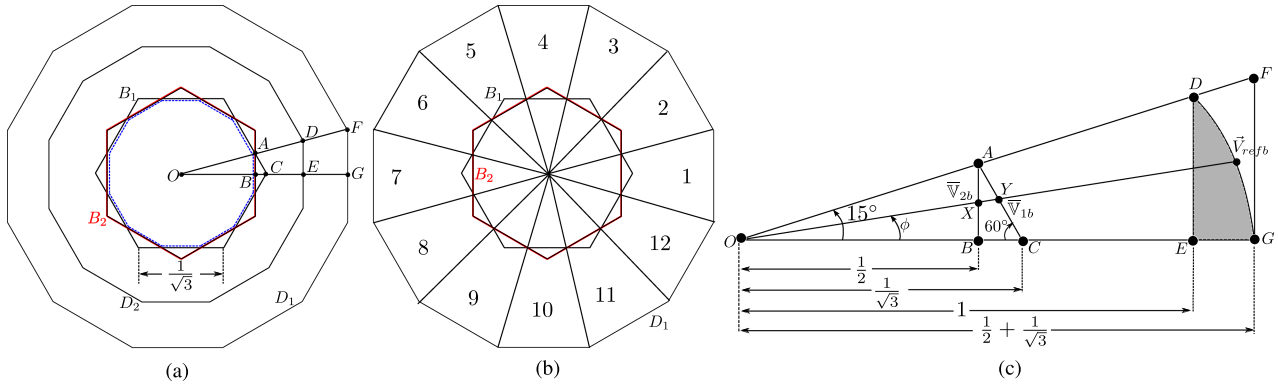

Fig. 5. Proposed OVM technique. (a) Boundaries of $\overline{\mathbb{V}}_1$, $\overline{\mathbb{V}}_2$, and $\overline{\mathbb{V}}_1 + \overline{\mathbb{V}}_2$. (b) Twelve sectors in $\alpha - \beta$. (c) Region of OVM of the proposed technique for $0 \leq \theta \leq 15^\circ$.

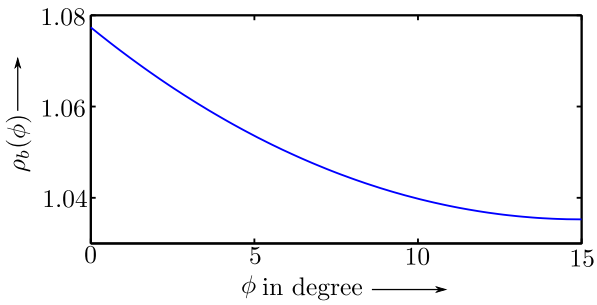

Fig. 6. $\rho_b(\phi)$ as function of ϕ with $V_{\text{DC}} = 1$.

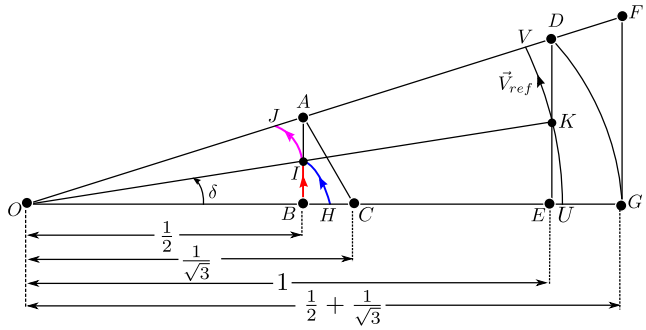

Fig. 7. $\overline{\mathbb{V}}_1$ and $\overline{\mathbb{V}}_2$ in the proposed technique for $0^\circ \leq \theta \leq 15^\circ$ and $M \in (0.577, 0.5977)$.

among the vectors whose tips lie on the curve DG. Therefore, the maximum length of the voltage vector that is possible to synthesize for all possible angles ($0^\circ \leq \theta_m \leq 15^\circ$) is OD and the maximum modulation index attainable with this strategy can be obtained by equating the absolute value of the circular reference voltage vector of (5) with OD. As $V_o = MV_{\text{DC}}$ and all lengths are scaled with a factor $\frac{1}{V_{\text{DC}}}$, reference voltage vector of (5) in modulo sector becomes $\vec{V}_{\text{ref},m} = \sqrt{3}Me^{j\theta_m}$, where θ_m is the angle in modulo sector. Therefore, the maximum modulation index, $M_{\text{max}} = \frac{\rho_b(15^\circ)}{\sqrt{3}} = \frac{1}{\sqrt{3}\cos 15^\circ} = 0.5977$, can be derived analytically.

A. Modulation Strategy

When M lies within the range $0 \leq M \leq 0.577$, tip of $\vec{V}_{\text{ref},m}$ always lie within ΔODE and, therefore, TINV-based linear modulation strategy, as discussed in Section III-A, will be adopted. For $0.577 \leq M \leq 0.5977$, tip of $\vec{V}_{\text{ref},m}$ lies partially outside ΔODE but within area ODG, as shown by curve UV in Fig. 7. Let, $\vec{V}_{\text{ref},m}$ intersects the line DE at K at an angle δ and, therefore, $\sqrt{3}M\cos\delta = OE = 2OB = 1$, which gives

$$\delta = \cos^{-1}\left(\frac{1}{\sqrt{3}M}\right). \tag{17}$$

So, δ is function of M alone. For $0^\circ \leq \theta_m \leq \delta$, $\vec{V}_{\text{ref},m}$ (UK) lies outside ΔODE. To satisfy (15a) with the adopted strategy ($\phi_1 = \phi_2$), following equation needs to be solved:

$$\overline{\mathbb{V}}_{1m} + \overline{\mathbb{V}}_{2m} \triangleq \rho_1 e^{j\phi_1} + \rho_2 e^{j\phi_2} = \vec{V}_{\text{ref},m} = \sqrt{3}Me^{j\theta_m}$$

which gives

$$\phi_1 = \theta_m = \phi_2 \tag{18a}$$

$$\rho_1 + \rho_2 = \sqrt{3}M. \tag{18b}$$

There are four unknowns and three equalities in the aforementioned equation. Therefore, we have 1 DOF. It can be seen from (15b) that the vector length applied in $z_1 - z_2$ plane can be minimized by minimizing $|\overline{\mathbb{V}}_1 - \overline{\mathbb{V}}_2|$. Therefore, the aforementioned degree of freedom can be utilized in order to choose $\rho_{1,2}$ for minimizing $|\overline{\mathbb{V}}_{1m} - \overline{\mathbb{V}}_{2m}|$. With $\phi_1 = \phi_2$, minimization of $|\overline{\mathbb{V}}_{1m} - \overline{\mathbb{V}}_{2m}|$ becomes equivalent to minimization of $|\rho_1 - \rho_2|$. To minimize $|\rho_1 - \rho_2|$, $\overline{\mathbb{V}}_{1m}$ and $\overline{\mathbb{V}}_{2m}$ should be as close as possible. When $\overline{\mathbb{V}}_{1m} = \overline{\mathbb{V}}_{2m}$ and both move along BA, we get ED in $\alpha - \beta$ plane. Therefore, to attain voltage vector beyond ED keeping $|\rho_1 - \rho_2|$ minimum, $\overline{\mathbb{V}}_{2m}$ should lie on its boundary, i.e., BA. Hence, for $0^\circ \leq \theta_m \leq \delta$ (UK part), $\overline{\mathbb{V}}_{2m}$ moves along BI (locus is shown by red color), which gives $\rho_2 = \frac{OB}{\cos\phi_2} = \frac{1}{2\cos\theta_m}$. To satisfy (18b), $\rho_1 = (\sqrt{3}M - \frac{1}{2\cos\theta_m})$ and $\overline{\mathbb{V}}_{1m}$ moves along HI in Fig. 7. In KV part, $\vec{V}_{\text{ref},m}$ lies within ΔADE and $\rho_1 = \rho_2$ will give zero voltage injection in $z_1 - z_2$ plane. Therefore, for $\delta \leq \theta_m \leq 15^\circ$, $\overline{\mathbb{V}}_{1m} = \overline{\mathbb{V}}_{2m} = \frac{\vec{V}_{\text{ref},m}}{2}$ and both of them move along circular arc IJ.

This modulation strategy is summarized for $0^\circ \leq \theta_m \leq 15^\circ$ in the $\alpha-\beta$ plane, as follows. When tip of $\vec{V}_{\text{ref},m}$ lies within ΔODE, it is in linear region and solution is given by (19). If tip of $\vec{V}_{\text{ref},m}$ lies within area EDG, it is in OVM and solution is given by (20). One of the ways to determine the linear or OVM region is to check whether $\theta_m \lesseqgtr \delta$, where δ is given in (17). Another way is to check whether $\overline{v}_{\alpha m} \lesseqgtr OE = 1$. In most of the applications, input to the PWM modulator is $(\overline{v}_\alpha, \overline{v}_\beta)$, instead of (M, θ). Therefore, solutions in (19) and (20) are given in terms of both $(\overline{v}_{\alpha m}, \overline{v}_{\beta m})$ and (M, θ_m)

$$\overline{\mathbb{V}}_{1m} = \overline{\mathbb{V}}_{2m} = \frac{\vec{V}_{\text{ref},m}}{2} \triangleq \frac{\overline{v}_{\alpha m}}{2} + j\frac{\overline{v}_{\beta m}}{2} \tag{19}$$

$$\overline{\mathbb{V}}_{2m} = \frac{1}{2\cos\theta_m} e^{j\theta_m} = \frac{1}{2} + j\frac{1}{2}\tan\theta_m = \frac{1}{2} + j\underbrace{\frac{1}{2}\frac{\overline{v}_{\beta m}}{\overline{v}_{\alpha m}}}_{y_{2m}}$$

$$\overline{\mathbb{V}}_{1m} = \left(\sqrt{3}M - \frac{1}{2\cos\theta_m}\right) e^{j\theta_m} = \vec{V}_{ref,m} - \overline{\mathbb{V}}_{2m}$$

$$= \left(\overline{v}_{\alpha m} - \frac{1}{2}\right) + j(\overline{v}_{\beta m} - y_{2m}). \tag{20}$$

Aforementioned solutions, which are given in terms of $(\overline{v}_{\alpha m}, \overline{v}_{\beta m})$, are also valid for lower half of sector-1 ($-15^\circ \leq \theta \leq 0^\circ$ in $\alpha-\beta$ plane). Solutions for kth sector, where $k \in \{1, 2, ..12\}$, are derived from (19) and (20) as follows. If $(\overline{v}_\alpha, \overline{v}_\beta)$ are given, k can be identified and subsequently, corresponding modulo-sector voltages can be determined by applying rotational transformation of (21). From this $(\overline{v}_{\alpha m}, \overline{v}_{\beta m})$, $\overline{\mathbb{V}}_{1m}$ and $\overline{\mathbb{V}}_{2m}$ are determined from (19) or (20) depending upon $\overline{v}_{\alpha m} \lesseqgtr 1$. If $\overline{v}_{\alpha m} > 1$, $\overline{\mathbb{V}}_{2m}$ moves along its boundary (BI in Fig. 7) as boundary of $\overline{\mathbb{V}}_2$, B_2, is within the boundary of $\overline{\mathbb{V}}_1$, B_1, in modulo sector. From Fig. 5(b), one can see that this is true for all odd sectors. In even sectors, B_1 lies within B_2. Based on this observation, reference voltage vectors per three-phase inverters can be determined from (22), where $x = 1$ and $y = 2$ when k is odd; $x = 2$ and $y = 1$ when k is even. Applying inverse transformation of (7a), modulation signals, $\overline{v}_{po}$ and $\overline{v}_{p'o'}$ where $p \in \{a, b\}$, can be derived. Combining (19), (20)–(22), and inverse transformation of (7a), final expressions of these modulating signals are given in (26)–(28) in the Appendix

$$\overline{v}_{\alpha m} + j\overline{v}_{\beta m} = (\overline{v}_\alpha + j\overline{v}_\beta)\, e^{-j(k-1)30^\circ}$$

$$\overline{v}_{\alpha m} = \overline{v}_\alpha \cos(k-1)30^\circ + \overline{v}_\beta \sin(k-1)30^\circ \tag{21a}$$

$$\overline{v}_{\beta m} = -\overline{v}_\alpha \sin(k-1)30^\circ + \overline{v}_\beta \cos(k-1)30^\circ \tag{21b}$$

$$\left(\overline{v}_{\underline{\alpha}} + j\overline{v}_{\underline{\beta}}\right) \triangleq \overline{\mathbb{V}}_1 = \overline{\mathbb{V}}_{xm} e^{j(k-1)30^\circ}$$

$$\left(\overline{v}_{\underline{\alpha'}} + j\overline{v}_{\underline{\beta'}}\right) \triangleq \overline{\mathbb{V}}_2 e^{-j30^\circ} = \overline{\mathbb{V}}_{ym} e^{j(k-2)30^\circ}. \tag{22}$$

B. Derivation of Harmonic Components of the Line-Neutral Voltages

The harmonic components of the line-neutral voltages resulted due to voltage injection in $z_1 - z_2$ plane will be derived in this section. The applied voltages in $\alpha-\beta$ subspace do not contain any harmonics. The voltage injection in $z_1 - z_2$ plane can be determined using (15b) from the knowledge of $\overline{\mathbb{V}}_1$ and $\overline{\mathbb{V}}_2$ [(19) and (20)]. These voltage expressions for $0^\circ \leq \theta \leq 360^\circ$ are given in (29) and (30) in the Appendix, where $k \in \{0, 1, ...5\}$. The harmonic components of $\overline{v}_{z_{1,2}}$ can be obtained using Fourier series analysis. The inverse transformation of (1) enables us to express the line-neutral voltages in the original domains in terms of voltages in transformed domains. Equation (23) expresses a-phase voltage. As $\overline{v}_{o_{1,2}} = 0$ and $\overline{v}_\alpha$ does not have any harmonics, therefore the harmonics present in $\overline{v}_{z_1}$ will appear in $\overline{v}_{ao}$ with a scaling factor of $\frac{1}{\sqrt{3}}$. The analytical closed-form expression of nth harmonic components of $\overline{v}_{ao}$ is given in (31) in the Appendix. The order of harmonics present in the line-neutral voltages is $n = 5, 7, 17, 19, ...12m \pm 5$ and the coefficients of (31) become zero for other odd harmonics. It is difficult to give a generalized expression for $\int_0^\delta \tan\theta \sin(n\theta) d\theta$ in terms of n and δ. Compared to other harmonics present in the line-neutral voltages, impacts of fifth and seventh harmonics are significant due to low impedance of equivalent circuit in $z_1 - z_2$ plane. Therefore, results of this definite integration for $n = 5$ and $n = 7$ are given in (32) and (33) in terms of δ. For a given M, one can obtain the analytical estimation of fifth and seventh harmonics present in the line-neutral voltages by using (17), (31)–(33). As $\overline{v}_\alpha(\theta) = \overline{v}_\beta(\theta + 90^\circ)$ and $\overline{v}_{z_1}(\theta) = \overline{v}_{z_2}(\theta + 90^\circ)$, it is possible to show that the other line-neutral voltages will have odd harmonics spectra similar to $\overline{v}_{ao}$

$$\overline{v}_{ao} = \frac{1}{\sqrt{3}}(\overline{v}_\alpha + \overline{v}_{z_1} + \overline{v}_{o_1}). \tag{23}$$

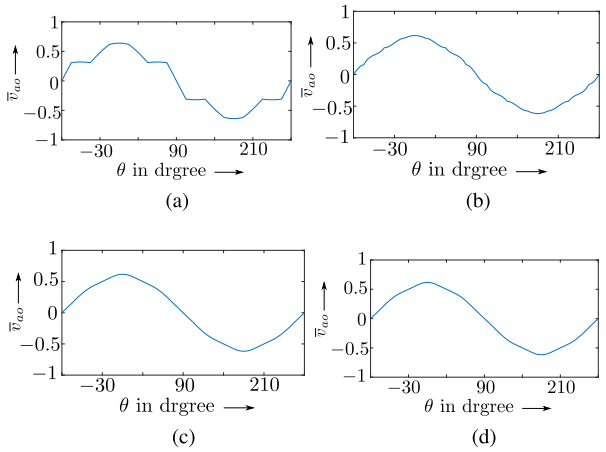

Fig. 8. Comparison of modulating signals at $M = 0.597$. (a) *CSVPWM*. (b) *SVOVM4-1*. (c) *SVOVM4-2*. (d) Proposed technique.

C. Comparisons of Modulation Techniques Based on Analysis

Figs. 8 and 9 compare the modulation signals $\overline{v}_{ao}$ and $\overline{v}_{z_1}$, respectively, of the proposed technique and the existing OVM techniques of ASIM at $M = 0.597$. In Fig. 8, the proposed strategy has almost similar waveform to *SVOVM4-2* and both of these strategies have less distortion compared to *SVOVM4-1* and *CSVPWM*. As $\overline{v}_{z_1}(\theta) = \overline{v}_{z_2}(\theta + 90^\circ)$, waveform of $\overline{v}_{z_2}$ is not shown. Voltage injection by *CSVPWM* in $z_1 - z_2$ plane is significantly higher compared to other three techniques and it

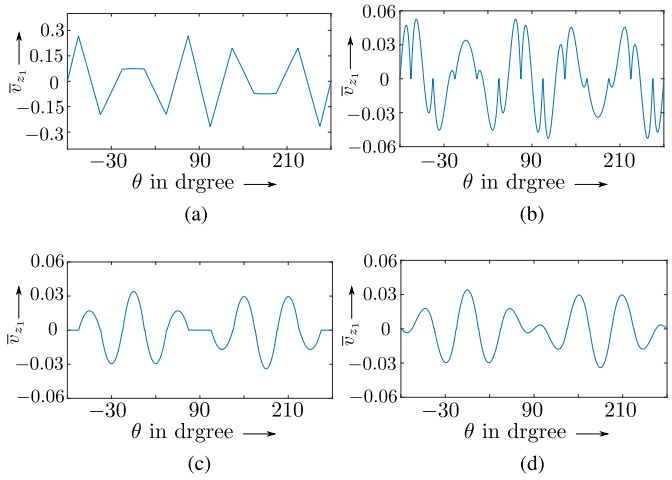

Fig. 9. Comparison of $\overline{v}_{z_1}$ at $M = 0.597$. (a) *CSVPWM*. (b) *SVOVM4-1*. (c) *SVOVM4-2*. (d) Proposed technique.

TABLE II
COMPARISON OF HARMONIC PERFORMANCES *CSVPWM* WITH OTHER THREE TECHNIQUES AT $M = 0.597$ (IN %)

	5^{th}	7^{th}	THD	WTHD
CSVPWM	8.8	4.36	16.55	3.13
SVOVM4-1	2.15	0.40	4.03	0.73
SVOVM4-2	1.08	0.91	2.38	0.42
Proposed technique	1.01	1.01	2.39	0.41

is plotted in different scale in Fig. 9. Among the rest three techniques, $\overline{v}_{z_1}$ of *SVOVM4-2* and the proposed technique are almost similar and they are better compared to *SVOVM4-1*. $\overline{v}_{z_1}$ of *SVOVM4-2* is zero for some θ, whereas it is nonzero in case of the proposed technique at $M = 0.597$. Although the proposed technique or *SVOVM4-1*, *SVOVM4-2* try to minimize THD in line-neutral voltages in order to minimize the injected voltage in $z_1 - z_2$, the main objective is to reduce the current THD in order to reduce the copper loss in $z_1 - z_2$ plane. As leakage inductance becomes predominant over winding resistance for higher order harmonics, therefore current THD reduction is equivalent to reduction of weighted THD (WTHD) whose expression is given as follows:

$$\text{WTHD} = \frac{\sqrt{\sum_{n=12m\pm5}(\frac{\overline{v}_{ao|n}}{n})^2}}{V_o}.$$

The harmonic performance of *CSVPWM* is worse by several orders compared to other three techniques over the entire range of $0.577 \leq M \leq 0.597$. Table II compares fifth harmonic, seventh harmonic, THD, and WTHD of line-neutral voltages of all four techniques at $M = 0.597$. Therefore, Fig. 10 compares those three techniques that have comparable harmonic performances. Harmonics up to hundredth order have been considered for the computation of WTHD. Fifth harmonic performance of the proposed technique is better than *SVOVM4-1* and *SVOVM4-2*, whereas *SVOVM4-1* is the best technique in terms of seventh harmonic injection. THD and WTHD performances of the proposed technique and *SVOVM4-2* are almost similar and they are better compared to *SVOVM4-1*. THD performance

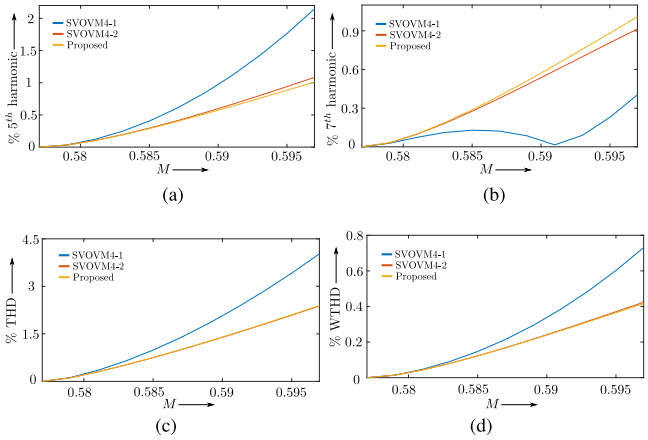

Fig. 10. Comparison of harmonic performances. (a) Fifth harmonics. (b) Seventh harmonics. (c) Voltage THD. (d) Voltage WTHD.

of *SVOVM4-2* is marginally better than the proposed technique, whereas WTHD performance of proposed technique is better compared to *SVOVM4-2* at higher M. As WTHD is the indicator of copper loss, the proposed technique will give the lowest copper loss among all four OVM techniques, as we will see in Section VII.

D. Comparisons of Two-Level 6ϕ Inverter Fed ASIM and Three-Level Neutral-Point-Clamped (NPC) Fed 3ϕ IM

As both multiphase machine and multilevel converter configurations lead to reduction of voltage stress of the devices, which is useful in medium-voltage high-power drives, comparison of these two configurations is important. For a given IM of rated power, it can be shown that the blocking voltage rating of the 12 switches in two-level 6ϕ inverter fed ASIM configuration with proposed technique is lesser than that of three-level NPC inverter fed 3ϕ IM configuration. Current ratings of both the configurations are same. The later needs six additional clamping diodes. In case of fault in one phase, the derating factors of ASIM and 3ϕ IM are $\frac{1}{6}$ and $\frac{1}{3}$, respectively, which show that fault tolerance of two-level 6ϕ inverter fed ASIM is higher as compared to three-level NPC fed 3ϕ IM.

VI. IMPLEMENTATION STRATEGY AND COMPUTATIONAL BURDEN OF THE PROPOSED TECHNIQUE

Following steps are required in order to determine six duty ratios of top switches of six half-bridge legs of Fig. 1 from the given $\overline{v}_\alpha$ and $\overline{v}_\beta$ pair. By comparing these duty ratios with triangular carrier, PWM modulator block generates six gating pulses of top six switches and six complemented gating pulses with fixed dead-time for bottom switches.

1) *Step 1. Sector Identification:* Depending upon signs of $\overline{v}_\alpha$ and $\overline{v}_\beta$, the reference voltage vector, $\vec{V}_{\text{ref}} \triangleq \overline{v}_\alpha + j\overline{v}_\beta$, may lie in one of the four quadrants in $\alpha - \beta$ plane. Each quadrant consists of four sectors, as shown in Fig. 5(b). Maximum three inequalities need to be checked for identifying the exact sector within one quadrant. For example, following inequalities need to be checked sequentially

from $l = 0$ to $l = 2$ to identify the sector in first quadrant:

$$\overline{v}_\beta \le \overline{v}_\alpha \tan((2l+1)15^\circ); \quad l \in \{0,1,2\}.$$

Two comparisons (COMPs) are required to determine the quadrant and maximum three multiplications (MULs) and three COMPs are required to check the three inequalities within a quadrant. Once the sector k is identified, remaining calculations are performed in the corresponding sector within if-else block.

2) *Step 2. Region Identification:* After identifying k, rotational transformation of (21) is applied to find $\overline{v}_{\alpha m}$ as follows:

$$\overline{v}_{\alpha m} = \overline{v}_\alpha \cos((k-1)30^\circ) + \overline{v}_\beta \sin((k-1)30^\circ).$$

If $\overline{v}_{\alpha m} \le 1$, $\vec{V}_{\text{ref}}$ is in linear region. Otherwise, it is in OVM region. Maximum two MULs, one addition (ADD), and one COMP are required to identify the region.

3) *Step 3. Determination of Modulation Signals:* Based on linear or OVM region of operation and k, four modulation signals can be calculated, which are given in (26)–(28) in the Appendix. Seven MULs and three ADDs/subtractions (SUBs) are required to compute four modulation signals in linear region. In OVM region, $\overline{v}_{\beta m}$ is calculated first from (21). Similar to $\overline{v}_{\alpha m}$ calculation, it requires two MULs and one ADD. With predetermined $\overline{v}_{\alpha m}$ and $\overline{v}_{\beta m}$, y_{2m}, which is given in (20), is evaluated by one division (DIV) and one MUL. The coefficients in (27) or (28) are constant numbers for a given k, therefore, they need not to be calculated online or stored in a table. After y_{2m} is calculated, maximum four MULs and seven ADDs/SUBs are required to compute four modulation signals from (27) or (28) at any sector k. Although this is not obvious from (27) and (28), one can see after plugging any k within $\{1, 2..12\}$ that few coefficients of (27) and (28) become either 1 or 0 and only aforementioned computations are required. For two isolated neutral connection, as shown in Fig. 1, $\overline{v}_{co}$ and $\overline{v}_{c'o'}$ can be calculated as (24) and additional two ADDs/SUBs are required to do so

$$\overline{v}_{co} = -(\overline{v}_{ao} + \overline{v}_{bo}); \quad \overline{v}_{c'o'} = -(\overline{v}_{a'o'} + \overline{v}_{b'o'}). \tag{24}$$

4) *Step 4. Determination of Duty Ratios:* This article uses $\frac{1}{2} + \frac{\text{mid}}{2}$ common mode voltages per three-phase inverters. Therefore, six duty ratios are calculated as (25). Here, $x \in \{a,b,c\}$ and $y \in \{a',b',c'\}$, mid and mid$'$ are the middle values of three modulation signals of two three-phase inverters, respectively. Maximum six COMPs are required to determine mid and mid$'$ and eight ADDs, two MULs, and two assign operations are required to calculate all duty ratios

$$d_x = \overline{v}_{xo} + (1 + \text{mid})\frac{1}{2}; \quad d_y = \overline{v}_{yo'} + (1 + \text{mid}')\frac{1}{2}. \tag{25}$$

Fig. 11 shows the algorithm to implement the proposed strategy in flowchart format. The computational burden of the aforementioned steps is shown in Table III.

When the computational burden of OVM techniques of ASIM is compared, it is seen that *CSVPWM* needs lowest computation as it is devoid of calculation of $z_1 - z_2$ plane voltages. But, *CSVPWM* causes substantially higher copper loss, as we will see in Section VII, and therefore, it is needless to compare with the proposed technique. As *SVOVM4-1* and *SVOVM4-2* have harmonic performance comparable to the proposed technique, they are compared. It is mentioned in [10] that offline calculated lookup table based *SVOVM4-1* and *SVOVM4-2* do not have any significant difference in execution time. Therefore, computational burden of *SVOVM4-2* is compared with the proposed technique. The scaling factor of transformation matrix used by Zhou *et al.* [10] is different from (1). For the sake of continuity, all the expressions related to *SVOVM4-2* are re-evaluated with respect to (1) in the following discussion.

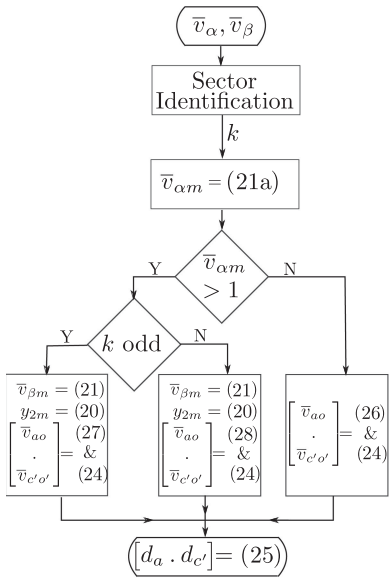

Fig. 11. Flowchart of the proposed strategy.

TABLE III
COMPARISON OF COMPUTATIONAL BURDENS OF THE PROPOSED TECHNIQUE AND *SVOVM4-2*

	ADD/SUB		MUL/DIV		COMP	
	Proposed	*SVOVM4-2*	Proposed	*SVOVM4-2*	Proposed	*SVOVM4-2*
Step-1	0	0	3	3	5	5
Step-2	1	3	2	5	1	3
Step-3	10	19	8	17	0	0
Step-4	8	8	2	2	6	6
Total	19	30	15	27	12	14

The implementation strategy of *SVOVM4-2* is discussed in [10].

1) Sector identification (step 1), same as discussed before, is required to determine k.
2) The second step, i.e., region identification, consists of two substeps, which are as follows.
   a) Calculation of $\overline{v}_{\alpha,\beta m}$ from the given $\overline{v}_{\alpha,\beta}$ using (21), which requires four MULs and two ADDs.
   b) Zone identification based on $\overline{v}_{\alpha,\beta m}$.

   If $\overline{v}_{\alpha m} > 1$, it is in OVM region. The OVM region in sector-1 is divided into three zones. Based on $\overline{v}_{\beta m} \lessgtr 0$

TABLE IV
STEADY-STATE EQUIVALENT CIRCUIT PARAMETERS OF ASIM

Per phase stator and rotor resistances	0.675 Ω
Per phase stator and rotor leakage inductances	3.75 mH
Per phase magnetizing inductance	0.168 H

and $2\sqrt{3}\overline{v}_{\alpha m} \pm \overline{v}_{\beta m} > (2+\sqrt{3})$ inequalities are satisfied or not, zone is identified. It requires one MUL, one ADD/SUB, and three COMPs. Therefore, step 2 requires five MULs, three ADD/SUBs, and three COMPs.

3) The third step, determination of modulation signals, consists of three substeps, which are as follows.
   a) Calculation of $\overline{v}_{z_1 m}$ and $\overline{v}_{z_2 m}$: In OVM, $\overline{v}_{z_1 m} = \overline{v}_{\alpha m} - 1$. In zone-1, $\overline{v}_{z_2 m} = 0$. In zone-2 and zone-3, $\overline{v}_{z_2 m} = \pm 2\sqrt{3}\overline{v}_{\alpha} + \overline{v}_{\beta} \mp (2+\sqrt{3})$. Therefore, maximum three ADD/SUBs and one MULs are required.
   b) Find $\overline{v}_{z_{1,2}}$ from $\overline{v}_{z_{1,2}m}$ using co-ordinate transformation $\overline{v}_{z_1} + j\overline{v}_{z_2} = (\overline{v}_{z_1 m} + j\overline{v}_{z_2 m})e^{j(k-1)150^\circ}$, which requires four MULs and two ADD/SUBs.
   c) From given $\overline{v}_{\alpha,\beta}$ and already calculated $\overline{v}_{z_{1,2}}$, six modulation signals are computed by taking inverse transformation of (1). The last two columns of the inverse matrix are not required as $\overline{v}_{o_{1,2}} = 0$. This substep requires 12 MULs and 14 ADD/SUBs. Therefore, step 3 requires 19 ADD/SUBs and 17 MULs.
4) Step 4, i.e., calculation of six duty ratios from modulation signals, is same as explained for the proposed algorithm. Computational burdens of these four steps are tabulated in Table III.

Comparing computational burdens in Table III, one can see that the proposed technique can be implemented up to $M = 0.5977$ at much reduced computational cost as compared to *SVOVM4-2* without compromising in performances, as can be seen from Fig. 10.

VII. EXPERIMENTAL AND SIMULATION RESULTS

A. Description of the Experimental Set-Up

A 5-kW, two-pole, 50 Hz squirrel-cage ASIM coupled with 5-kW dc generator (acts as load) has been used to validate the modulation strategy experimentally. The steady-state equivalent circuit parameters of this machine are shown in Table IV.A 1200-V, 75-A SEMIKRON IGBT (SKM75GB123D) based half-bridge module has been used to build the six-phase inverter. Zynq-7010 based controller platform is used to generate the PWM signals of the inverter. Zynq-7010 from Xilinx is a system on chip, which has both processor of dual-core ARM Cortex-A9 architecture (PS) as well as programmable logic (PL) cells, connected through parallel AXI bus. The clock frequency of the processor can go up to 866 MHz. PL has 28k logic cells, 2.1-Mb block RAM, 80 DSP slices, and 100 I/O pins. In this article, clock frequencies of PS and PL are set to 666 and 100 MHz, respectively. Fig. 12 shows the experimental set-up. The six-phase inverter drives the ASIM, which is coupled with a separately excited dc generator, which are shown separately

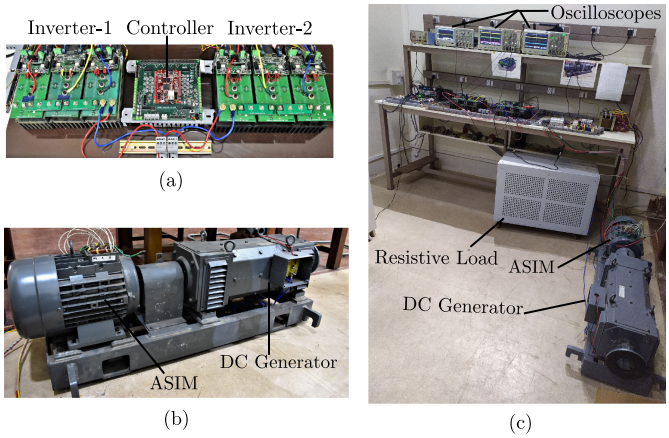

Fig. 12. Experimental set-up. (a) Six-phase inverter and controller. (b) ASIM couples with dc generator. (c) Overall set-up.

TABLE V
OPERATING CONDITIONS OF EXPERIMENTS AND SIMULATIONS

Peak fundamental line-neutral voltage (V_o)	$120\sqrt{2}$ V
Fundamental frequency (f_o)	50 Hz
Output power	4.2 kW
Switching frequency ($F_s = \frac{1}{T_s}$)	5 kHz

in Fig. 12(a) and (b). The rated output voltage of generator is 400 V and is connected across a resistive load bank. Tektronix MSO2024B, MDO3104 oscilloscopes, TCP0030A current probes, and P5200A differential voltage probes are used during experiment. The overall experimental set-up is shown in Fig. 12(c). To validate the proposed strategy in simulation, dynamic model of ASIM is developed in MATLAB Simulink using the circuit parameters of Table IV. The inverter is simulated using ideal switches. All the experimental and simulation results correspond to the operating conditions are shown in Table V. As $MV_{\text{DC}} = V_o = 120\sqrt{2} = 169.7$ V, dc-bus voltage V_{DC} has been changed for different M to keep their product constant.

B. Steady-State Results

Experiments have been performed at five M values spaced equally within $0.577 - 0.597$. Fig. 13 shows the experimental and simulated results at maximum M, i.e., $M = 0.597$. Fig. 13(c) shows the line–line voltages v_{ab} and $v_{a'b'}$, which are phase shifted by 30°. Simulated line–line voltages are shown in Fig. 13(f). Fig. 13(a) shows the phase currents i_a and $i_{a'}$ (phase shifted by 30° to each other), which closely matches with the simulated waveform shown in Fig. 13(d). Phase currents i_a, i_b, and i_c are balanced three-phase currents phase shifted by 120° to each other, as shown in Fig. 13(b) and (e). The other set of three-phase currents ($i_{a'}$, $i_{b'}$, $i_{c'}$) is similar but phase shifted by 30° with respect to the aforementioned set and, hence, is not shown. Fig. 13(g) and (h) shows the experimentally obtained currents in $\alpha - \beta$ and $z_1 - z_2$ planes, respectively. To obtain the currents in transformed domains, data points of experimentally obtained phase currents are saved in one excel file and subsequently,

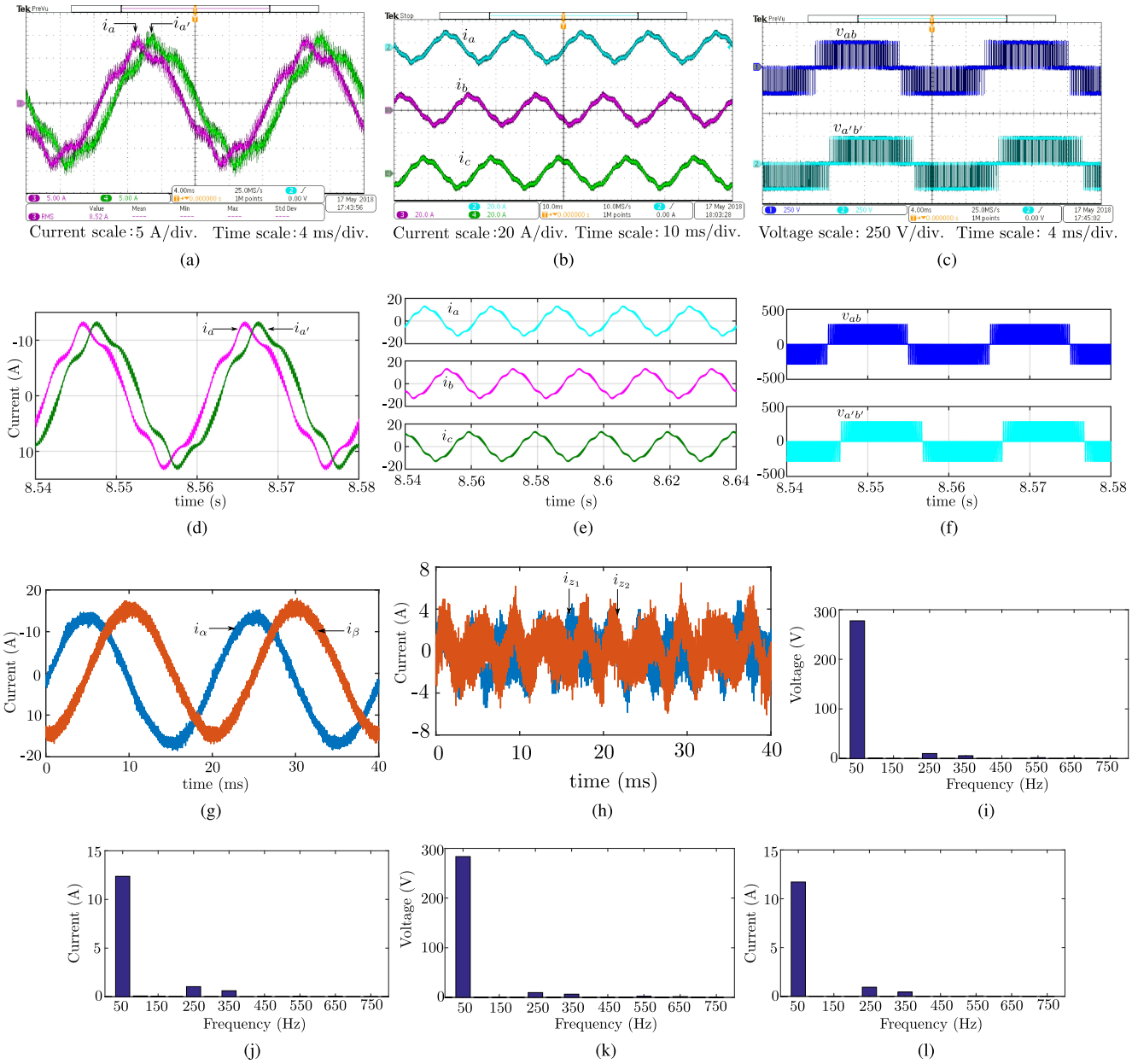

Fig. 13. Experimental and simulation results of the proposed technique at $M = 0.597$. (a) Experimental i_a and $i_{a'}$. (b) Experimental i_a, i_b, and i_c. (c) Experimental v_{ab} and $v_{a'b'}$. (d) Simulated i_a and $i_{a'}$. (e) Simulated i_a, i_b, and i_c. (f) Simulated v_{ab} and $v_{a'b'}$. (g) Experimental i_α and i_β. (h) Experimental i_{z_1} and i_{z_2}. (i) Spectrum of experimental v_{ab}. (j) Spectrum of experimental i_a. (k) Spectrum of simulated v_{ab}. (l) Spectrum of simulated i_a.

transformation T is applied on these data points in MATLAB. Currents in $\alpha - \beta$ plane are sinusoidal, as expected, due to the balanced sinusoidal voltage application in this plane and it validate the proposed strategy. The harmonic spectra of both line–line voltage and phase currents for the experimental and simulated waveforms are shown in Fig. 13(i), (k) and Fig. 13(j), (l), respectively, where the presence of fifth and seventh harmonics is prominent, as discussed in Section V-B. The peaks of the fundamental component of v_{ab} are 279.9 and 283.5 V in experimental and simulated results, which means, peaks of line-neutral voltages are 161.6 and 163.7 V, respectively. The peaks of fundamental component of i_a in experimental and simulated waveforms are 12.4 and 11.7 A, respectively.

TABLE VI
SIMULATION-BASED COMPARISON OF COPPER LOSSES IN $z_1 - z_2$ PLANE (IN WATT)

M	0.581	0.585	0.589	0.593	0.597
CSVPWM	41.04	41.01	41.06	40.98	40.84
SVOVM4-1	0.37	0.43	0.63	1.34	2.61
SVOVM4-2	0.42	0.47	0.68	0.98	1.42
Proposed technique	0.36	0.47	0.54	0.80	1.09

Table VI compares the simulation results of copper losses incurred in $z_1 - z_2$ plane for all four techniques at aforementioned

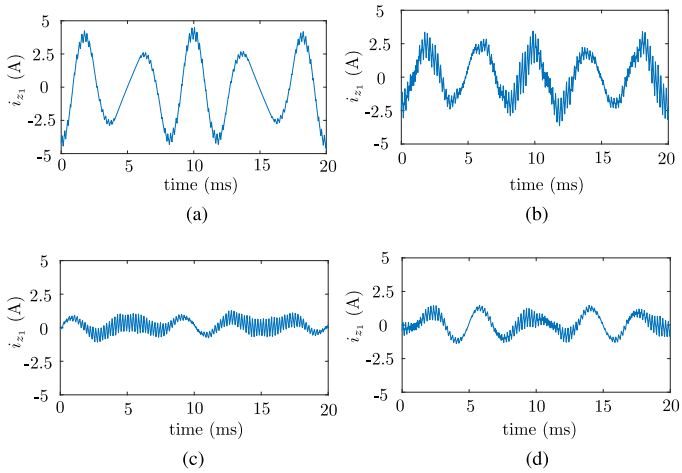

Fig. 14. Simulated i_{z_1} of four techniques at $M = 0.597$. (a) *CSVPWM*. (b) *SVOVM4-1*. (c) *SVOVM4-2*. (d) Proposed technique.

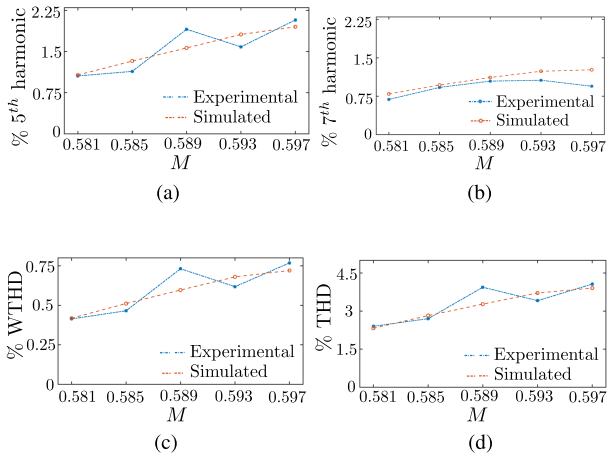

Fig. 15. Experimental and simulated harmonic performances for $0.577 < M \leq 0.597$. (a) Fifth harmonic as function of M. (b) Seventh harmonic as function of M. (c) WTHD as function of M. (d) THD as function of M.

five M using the machine parameters mentioned in Table IV. The proposed technique gives the lowest copper loss among these four techniques at higher M, which is close to the copper loss of *SVOVM4-2*. As this copper loss is related to current waveforms in $z_1 - z_2$ plane (copper loss is equal to $(i^2_{z_1,\text{RMS}} + i^2_{z_2,\text{RMS}}) \times r_s$, where $i_{z_1,\text{RMS}}$ and $i_{z_2,\text{RMS}}$ are rms values of i_{z_1} and i_{z_2}, respectively, and r_s is the resistance seen by the $z_1 - z_2$ plane), i_{z_1} plots for all four techniques at $M = 0.597$ are shown in Fig. 14, which validate Table VI. The waveform of i_{z_2} is similar to i_{z_1} but phase shifted by 90°, therefore, i_{z_2} plot is not shown here. Fig. 15 compares the performance of the proposed technique, as obtained through experiments and simulations, over the range $0.577 < M \leq 0.597$ at five distinct M values. Close agreements of THD, WTHD, fifth, and seventh harmonic performances between experimental and simulated waveforms validate the proposed strategy. The difference between analytical and experimental WTHD, THD, fifth, and seventh harmonic estimation arises due to the clamping of the duty ratios of the inverter switches at 0.975 (upper bound) and 0.025 (lower bound) for

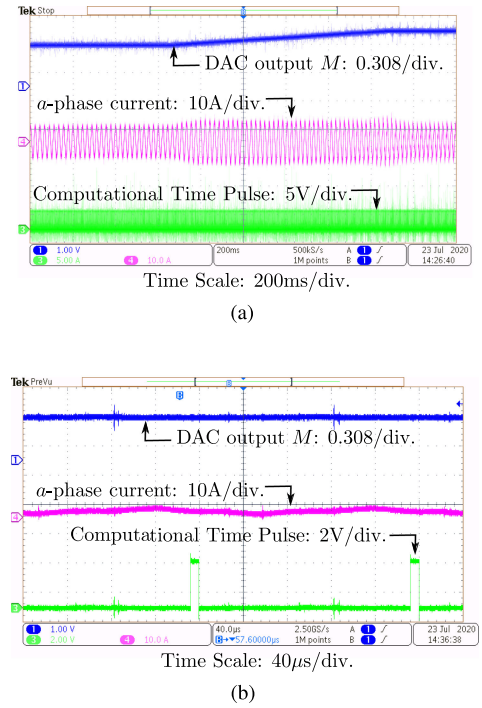

Fig. 16. Dynamic performance of ASIM and computation time of proposed strategy. (a) Open-loop V/f control: $M = 0.448$, $f_o = 45$ Hz to $M = 0.597$, $f_o = 50$ Hz. (b) Computational time of the proposed strategy.

proper dead-time operation between top and bottom switches of a leg. 1.2-μs dead-time is used between top and bottom switches of the inverter and if the switch "ON" time is less than 5 μs, the switch is kept in "OFF" state. When the duty ratios have not been clamped in simulation (it is possible as ideal switches are used in simulation), these performance indices are closely matching with the analytical results.

C. Results With Dynamics

Fig. 16(a) shows the dynamic performance of ASIM, driven by V/f control, where M (brought out from the controller through DAC), one of the line currents and computational time pulse, are captured in one scope. Computational time pulse is a signal that is high when the calculation of PWM modulator is in progress. During this experiment, M and output frequency f_o are changed from (0.448, 45 Hz) to (0.597, 50 Hz) in 1 s. It can be seen that the line current was going through a transient during the ramped increase in M, as expected, and settled back to its original state once the dynamics is over. Fig. 16(b) shows the zoomed version of Fig. 16(a) over few sampling cycles to show the computational time pulse. As expected, its frequency is same as the sampling frequency ($F_s = \frac{1}{T_s}$ =5 kHz), and computation time is 8 μs, which is much smaller than T_s=200 μs.

D. Closed-Loop Results

The closed-loop performances of scalar-controlled (V/f) ASIM have been simulated in MATLAB and shown in Fig. 17. The plant model is similar to 3ϕ IM where the steady-state torque is proportional to the slip speed. Proportional-integral

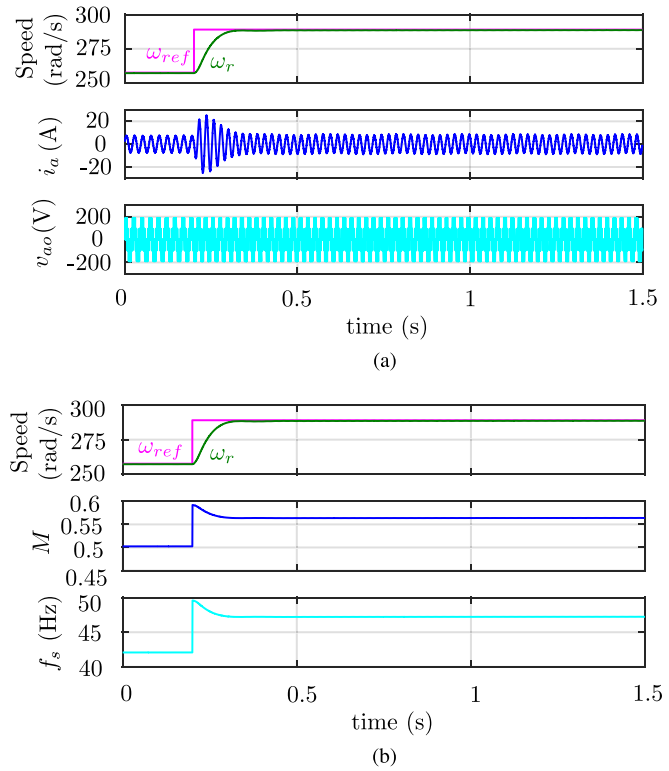

Fig. 17. Simulated scalar-controlled closed-loop response of ASIM. (a) ω_{ref}, ω_r, i_a, and v_{ao}. (b) ω_{ref}, ω_r, M, and f_s.

controller is designed such that the pole of the mechanical load is cancelled by the zero of the controller and the rise time of the resultant first order system is 0.15 s. This choice of rise time results into transient current to be 150% of full load current, which is in the permissible range [32]. Fig. 17(a) shows the closed-loop speed, voltage, and current waveforms when there is step change of reference speed from 258 to 289 rad/s. The changes in synchronous frequency f_s and M are shown in Fig. 17(b). (M, f_s) pair are changed from (0.5, 41.87 Hz), i.e., linear region, reach the peak of (0.592, 49.58 Hz), i.e., OVM region, and finally settled down to (0.564, 47.24 Hz).

VIII. Conclusion

This article derives an important relationship between individual space vectors of two three-phase inverters and the space vectors in $\alpha-\beta$ and z_1-z_2 subspaces of six-phase inverter. Using the aforementioned relation, an OVM technique is proposed, which modulates two three-phase inverters in order to synthesize the given reference voltage vector in $\alpha-\beta$ subspace. According to proposed strategy, the reference vectors of these two inverters are always phase shifted by 30°. As usual, in linear region, their magnitudes are same and equal to half of the magnitude of reference voltage vector in $\alpha-\beta$ subspace. But in OVM region, their magnitudes are different. The maximum modulation index achievable by this technique is derived analytically and found to be 0.5977. This technique does not inject any harmonics in $\alpha-\beta$ subspace and, therefore, no torque pulsation is created in ASIM. The proposed technique covers 44.44% of the entire OVM range. Analytical closed-form expression of harmonic components of the line-neutral voltages is derived. The proposed strategy injects $n=5,7,17,19,...12m\pm5$ order harmonics in line-neutral voltages. In OVM range, both THD and WTHD of the line-neutral voltages are monotonically increasing functions of modulation index and are 2.4% and 0.42%, respectively, at maximum modulation index. Detailed comparisons of harmonic performances of the proposed technique with other existing techniques reveal that THD, WTHD performances of the proposed technique is better than existing *CSVPWM* and *SVOVM4-1* techniques and almost similar to optimal *SVOVM4-2*, whereas comparison of computational burdens of the proposed technique with *SVOVM4-2* shows that the proposed technique can be implemented at much reduced computational cost without involving complex 6-D transformation. The proposed technique is validated through experiments and simulation on 4.2-kW hardware prototype.

Appendix

In linear region of operation ($\overline{v}_{\alpha m}\le 1$), (26) , as shown at the bottom of this page, gives the expressions for modulation signals. Equations (27) and (28) give the modulation signals of odd and even sectors, respectively, in OVM operation

$$\overline{v}_{ao}=\frac{1}{\sqrt{3}}\overline{v}_\alpha;\quad \overline{v}_{a'o'}=\frac{1}{2}\overline{v}_\alpha+\frac{1}{2\sqrt{3}}\overline{v}_\beta;\quad \overline{v}_{bo}=-\frac{1}{2\sqrt{3}}\overline{v}_\alpha+\frac{1}{2}\overline{v}_\beta;\quad \overline{v}_{b'o'}=-\frac{1}{2}\overline{v}_\alpha+\frac{1}{2\sqrt{3}}\overline{v}_\beta \tag{26}$$

$$\overline{v}_{ao}=\frac{2}{\sqrt{3}}\overline{v}_\alpha+\left(\frac{2}{\sqrt{3}}\sin\left((k-1)30^\circ\right)\right)y_{2m}-\frac{1}{\sqrt{3}}\cos\left((k-1)30^\circ\right);\quad \overline{v}_{a'o'}=\left(-\frac{2}{\sqrt{3}}\sin\left((k-2)30^\circ\right)\right)y_{2m}$$
$$+\frac{1}{\sqrt{3}}\cos\left((k-2)30^\circ\right)$$

$$\overline{v}_{bo}=-\frac{1}{\sqrt{3}}\overline{v}_\alpha+\overline{v}_\beta-\left(\frac{2}{\sqrt{3}}\sin\left((k+1)30^\circ\right)\right)y_{2m}+\frac{1}{\sqrt{3}}\cos\left((k+1)30^\circ\right);\quad \overline{v}_{b'o'}=\left(\frac{2}{\sqrt{3}}\sin\left(k30^\circ\right)\right)y_{2m}-\frac{1}{\sqrt{3}}\cos\left(k30^\circ\right) \tag{27}$$

$$\overline{v}_{ao}=\left(-\frac{2}{\sqrt{3}}\sin\left((k-1)30^\circ\right)\right)y_{2m}+\frac{1}{\sqrt{3}}\cos\left((k-1)30^\circ\right);\quad \overline{v}_{a'o'}=\overline{v}_\alpha+\frac{1}{\sqrt{3}}\overline{v}_\beta+\left(\frac{2}{\sqrt{3}}\sin\left((k-2)30^\circ\right)\right)y_{2m}$$
$$-\frac{1}{\sqrt{3}}\cos\left((k-2)30^\circ\right)$$

$$\overline{v}_{bo} = \left(\frac{2}{\sqrt{3}}\sin\left((k+1)30^\circ\right)\right) y_{2m} - \frac{1}{\sqrt{3}}\cos\left((k+1)30^\circ\right);$$

$$\overline{v}_{b'o'} = -\overline{v}_\alpha + \frac{1}{\sqrt{3}}\overline{v}_\beta - \left(\frac{2}{\sqrt{3}}\sin\left(k30^\circ\right)\right) y_{2m} + \frac{1}{\sqrt{3}}\cos\left(k30^\circ\right) \tag{28}$$

$$\overline{v}_{z_1} = \begin{cases} \left(\dfrac{1}{\cos\delta} - \dfrac{1}{\cos\left(\frac{k\pi}{3} - \theta\right)}\right)\cos\theta; & \left(\dfrac{k\pi}{3} - \delta\right) \le \theta \le \left(\dfrac{k\pi}{3} + \delta\right) \\ \left(\dfrac{1}{\cos\left(\frac{(2k+1)\pi}{6} - \theta\right)} - \dfrac{1}{\cos\delta}\right)\cos\theta; & \left(\dfrac{(2k+1)\pi}{6} - \delta\right) \le \theta \le \left(\dfrac{(2k+1)\pi}{6} + \delta\right) \\ 0; & \text{elsewhere} \end{cases} \tag{29}$$

$$\overline{v}_{z_2} = \begin{cases} \left(\dfrac{1}{\cos\delta} - \dfrac{1}{\cos\left(\frac{k\pi}{3} - \theta\right)}\right) - \sin\theta; & \left(\dfrac{k\pi}{3} - \delta\right) \le \theta \le \left(\dfrac{k\pi}{3} + \delta\right) \\ \left(\dfrac{1}{\cos\left(\frac{(2k+1)\pi}{6} - \theta\right)} - \dfrac{1}{\cos\delta}\right) - \sin\theta; & \left(\dfrac{(2k+1)\pi}{6} - \delta\right) \le \theta \le \left(\dfrac{(2k+1)\pi}{6} + \delta\right) \\ 0; & \text{elsewhere} \end{cases} \tag{30}$$

$$\begin{aligned} \overline{v}_{ao}|_n = \frac{4}{\sqrt{3}\pi}\Bigg[& \frac{1}{\cos\delta}\left(1 - \sqrt{3}\cos\left(\frac{n\pi}{6}\right) + \cos\left(\frac{n\pi}{3}\right)\right)\frac{n\cos\delta\sin(n\delta) - \sin\delta\cos(n\delta)}{n^2-1} \\ & + \frac{1}{\cos\delta}\left(-\sin\left(\frac{n\pi}{2}\right) + \sqrt{3}\sin\left(\frac{n\pi}{3}\right) - \sin\left(\frac{n\pi}{6}\right)\right) \\ & \frac{\cos\delta\sin(n\delta) - n\sin\delta\cos(n\delta)}{n^2-1} + \left(-1 + \sqrt{3}\cos\left(\frac{n\pi}{6}\right) - \cos\left(\frac{n\pi}{3}\right)\right)\frac{\sin(n\delta)}{n} \\ & + \left(\sin\left(\frac{n\pi}{2}\right) - \sqrt{3}\sin\left(\frac{n\pi}{3}\right) + \sin\left(\frac{n\pi}{6}\right)\right)\int_0^\delta \tan\theta\sin(n\theta)d\theta\Bigg] \end{aligned} \tag{31}$$

$$\int_0^\delta \tan\theta\sin(5\theta)d\theta = \left[-2\sin\delta + \frac{2}{3}\sin(3\delta) - \frac{1}{5}\sin(5\delta) + \ln\left(\tan\left(\frac{\pi}{4} + \frac{\delta}{2}\right)\right)\right] \tag{32}$$

$$\int_0^\delta \tan\theta\sin(7\theta)d\theta = \left[2\sin\delta - \frac{2}{3}\sin(3\delta) + \frac{2}{5}\sin(5\delta) - \frac{1}{7}\sin(7\delta) + \ln\left(\tan\left(\frac{\pi}{4} - \frac{\delta}{2}\right)\right)\right]. \tag{33}$$

ACKNOWLEDGMENT

The authors would like to thank Anirban Pal for the support and assistance provided to take some of the experimental results.

REFERENCES

[1] F. Barrero and M. J. Duran, "Recent advances in the design, modeling, and control of multiphase machines—Part I," *IEEE Trans. Ind. Electron.*, vol. 63, no. 1, pp. 449–458, Jan. 2016.

[2] E. Levi, "Advances in converter control and innovative exploitation of additional degrees of freedom for multiphase machines," *IEEE Trans. Ind. Electron.*, vol. 63, no. 1, pp. 433–448, Jan. 2015.

[3] K. Gopakumar, V. Ranganthan, and S. Bhat, "Split-phase induction motor operation from PWM voltage source inverter," *IEEE Trans. Ind. Appl.*, vol. 29, no. 5, pp. 927–932, Sep./Oct. 1993.

[4] D. Hadiouche, H. Razik, and A. Rezzoug, "On the modeling and design of dual-stator windings to minimize circulating harmonic currents for VSI fed ac machines," *IEEE Trans. Ind. Appl.*, vol. 40, no. 2, pp. 506–515, Mar./Apr. 2004.

[5] H. S. Che, A. S. Abdel-Khalik, O. Dordevic, and E. Levi, "Parameter estimation of asymmetrical six-phase induction machines using modified standard tests," *IEEE Trans. Ind. Electron.*, vol. 64, no. 8, pp. 6075–6085, Aug. 2017.

[6] Y. Zhao and T. A. Lipo, "Space vector PWM control of dual three-phase induction machine using vector space decomposition," *IEEE Trans. Ind. Appl.*, vol. 31, no. 5, pp. 1100–1109, Sep./Oct. 1995.

[7] D. Hadiouche, L. Baghli, and A. Rezzoug, "Space-vector PWM techniques for dual three-phase ac machine: Analysis, performance evaluation, and DSP implementation," *IEEE Trans. Ind. Appl.*, vol. 42, no. 4, pp. 1112–1122, Jul./Aug. 2006.

[8] K. Marouani, L. Baghli, D. Hadiouche, A. Kheloui, and A. Rezzoug, "A new PWM strategy based on a 24-sector vector space decomposition for a six-phase VSI-fed dual stator induction motor," *IEEE Trans. Ind. Electron.*, vol. 55, no. 5, pp. 1910–1920, May 2008.

[9] J. Prieto, J. A. Riveros, and B. Bogado, "Continuous and discontinuous SVPWM 2L+ 2M for asymmetrical dual three-phase drives," in *Proc. IEEE Int. Elect. Mach. Drives Conf.*, 2017, pp. 1–6.

[10] C. Zhou, G. Yang, and J. Su, "PWM strategy with minimum harmonic distortion for dual three-phase permanent-magnet synchronous motor drives operating in the overmodulation region," *IEEE Trans. Power Electron.*, vol. 31, no. 2, pp. 1367–1380, Feb. 2016.

[11] C. Wang, K. Wang, and X. You, "Research on synchronized SVPWM strategies under low switching frequency for six-phase VSI-fed asymmetrical dual stator induction machine," *IEEE Trans. Ind. Electron.*, vol. 63, no. 11, pp. 6767–6776, Nov. 2016.

[12] P. R. Rakesh and G. Narayanan, "Analysis of sine-triangle and zero-sequence injection modulation schemes for split-phase induction motor drive," *IET Power Electron.*, vol. 9, no. 2, pp. 344–355, 2016.

[13] H. Eldeeb, C. Hackl, M. Abdelrahem, and A. S. Abdel-Khalik, "A unified SVPWM realization for minimizing circulating currents of dual three phase machines," in *Proc. IEEE 12th Int. Conf. Power Electron. Drive Syst.*, 2017, pp. 925–931.
[14] J. Prieto, J. A. Riveros, and B. Bogado, "Multifrequency output voltage generation for asymmetrical dual three-phase drives," in *Proc. IEEE Int. Elect. Mach. Drives Conf.*, 2017, pp. 1–6.
[15] A. Bakhshai, G. Joos, and H. Jin, "Space vector PWM control of a split-phase induction machine using the vector classification technique," in *Proc. 13th Annu. Appl. Power Electron. Conf. Expo.*, 1998, vol. 2, pp. 802–808.
[16] R. Bojoi, A. Tenconi, F. Profumo, G. Griva, and D. Martinello, "Complete analysis and comparative study of digital modulation techniques for dual three-phase ac motor drives," in *Proc. IEEE 33rd Annu. Power Electron. Specialists Conf.*, 2002, vol. 2, pp. 851–857.
[17] D. Yazdani, S. A. Khajehoddin, A. Bakhshai, and G. Joos, "Full utilization of the inverter in split-phase drives by means of a dual three-phase space vector classification algorithm," *IEEE Trans. Ind. Electron.*, vol. 56, no. 1, pp. 120–129, Jan. 2009.
[18] H. S. Che, E. Levi, M. Jones, W.-P. Hew, and N. A. Rahim, "Current control methods for an asymmetrical six-phase induction motor drive," *IEEE Trans. Power Electron.*, vol. 29, no. 1, pp. 407–417, Jan. 2014.
[19] Y. Ren and Z.-Q. Zhu, "Reduction of both harmonic current and torque ripple for dual three-phase permanent-magnet synchronous machine using modified switching-table-based direct torque control," *IEEE Trans. Ind. Electron.*, vol. 62, no. 11, pp. 6671–6683, Nov. 2015.
[20] M. J. Duran, I. G. Prieto, M. Bermudez, F. Barrero, H. Guzman, and M. R. Arahal, "Optimal fault-tolerant control of six-phase induction motor drives with parallel converters," *IEEE Trans. Ind. Electron.*, vol. 63, no. 1, pp. 629–640, Jan. 2015.
[21] M. J. Duran and F. Barrero, "Recent advances in the design, modeling, and control of multiphase machines—Part II," *IEEE Trans. Ind. Electron.*, vol. 63, no. 1, pp. 459–468, Jan. 2016.
[22] W. N. W. A. Munim, M. J. Duran, H. S. Che, M. Bermúdez, I. González-Prieto, and N. A. Rahim, "A unified analysis of the fault tolerance capability in six-phase induction motor drives," *IEEE Trans. Power Electron.*, vol. 32, no. 10, pp. 7824–7836, Oct. 2017.
[23] G. K. Singh, K. Nam, and S. Lim, "A simple indirect field-oriented control scheme for multiphase induction machine," *IEEE Trans. Ind. Electron.*, vol. 52, no. 4, pp. 1177–1184, Aug. 2005.
[24] D. G. Holmes and T. A. Lipo, *Pulse Width Modulation for Power Converters: Principles And Practice*, vol. 18. Hoboken, NJ, USA: Wiley, 2003.
[25] A. Iqbal and E. Levi, "Space vector modulation schemes for a five-phase voltage source inverter," in *Proc. Eur. Conf. Power Electron. Appl.*, Dresden, 2005, p. 12, doi: 10.1109/EPE.2005.219194.
[26] J. Prieto, F. Barrero, M. J. Durán, S. T. Marín, and M. A. Perales, "SVM procedure for n-phase VSI with low harmonic distortion in the overmodulation region," *IEEE Trans. Ind. Electron.*, vol. 61, no. 1, pp. 92–97, Jan. 2014.
[27] G. Carrasco and C. A. Silva, "Space vector PWM method for five-phase two-level VSI with minimum harmonic injection in the overmodulation region," *IEEE Trans. Ind. Electron.*, vol. 60, no. 5, pp. 2042–2053, May 2013.
[28] M. J. Duran, J. Prieto, and F. Barrero, "Space vector PWM with reduced common-mode voltage for five-phase induction motor drives operating in overmodulation zone," *IEEE Trans. Power Electron.*, vol. 28, no. 8, pp. 4030–4040, Aug. 2013.
[29] T. Komrska, T. Glasberger, and Z. Peroutka, "Universal PWM modulator for multiphase drives with a minimum infinity-norm approach," *IEEE Trans. Ind. Electron.*, vol. 63, no. 10, pp. 5979–5987, Oct. 2016.
[30] J. Holtz, W. Lotzkat, and A. M. Khambadkone, "On continuous control of PWM inverters in the overmodulation range including the six-step mode," *IEEE Trans. Power Electron.*, vol. 8, no. 4, pp. 546–553, Oct. 1993.
[31] D. White and H. Woodson, *Electromagnetic Energy Conversion*. Hoboken, NJ, USA: Wiley, 1959.
[32] N. Mohan, *Electric Drives: An Integrative Approach*. Minneapolis, MN, USA: MNPERE, 2001.

Sayan Paul received the B.Tech. degree in electrical engineering from the National Institute of Technology, Durgapur, India, in 2014, and the M.Eng. degree in electrical engineering in 2018 from the Indian Institute of Science, Bangalore, India, where he is currently working toward the Ph.D. degree with the Department of Electrical Engineering.

His research interests include PWM techniques, modeling and control of multiphase drives, and multilevel converters.

Kaushik Basu (Senior Member, IEEE) received the B.E. degree from the Bengal Engineering and Science University, Howrah, India, in 2003, the M.S. degree in electrical engineering from the Indian Institute of Science, Bangalore, India, in 2005, and the Ph.D. degree in electrical engineering from the University of Minnesota, Minneapolis, MN, USA, in 2012.

He was a Design Engineer with Cold Watt India in 2006 and an Electronics and Control Engineer with Dynapower Corporation, South Burlington, VT, USA, from 2013 to 2015. He is currently an Assistant Professor with the Department of Electrical Engineering, Indian Institute of Science. He has authored or coauthored several technical papers published in peer-reviewed journals and conferences. His research interests include various aspects of the general area of power electronics.

Dr. Basu is the Founding Chair of the IEEE Power Electronics Society and IES Bangalore Chapter.